Quantum-cutting Luminescence in $CsPbCl_3$:Yb^{3+} Perovskite Nanocrystals

Master Thesis

Author: B.Sc. Jeffrey Zom
Daily supervisor: M.Sc. Mark J. J. Mangnus
Project supervisor: Dr. Freddy T. Rabouw

May 14, 2022

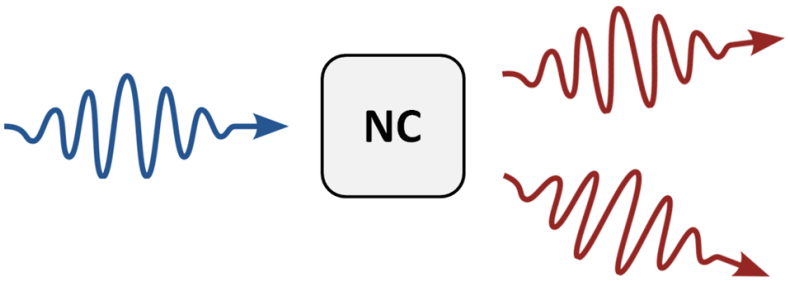

Department of Soft Condensed Matter, Utrecht Debye Institute, Utrecht University, Ornstein Laboratory, Princetonplein 1, 3508 TA Utrecht, The Netherlands

ABSTRACT: $CsPbCl_3$ perovskite nanocrystals doped with ytterbium have recently been discovered as highly efficient blue-to-NIR quantum-cutting phosphors. However, the quantum-cutting efficiency has been measured to decrease with increasing intensity of incident light. While $CsPbCl_3$:Yb^{3+} could increase the efficiency of photovoltaic devices, this saturation effect prevents effective application. Different mechanism for quantum-cutting and luminescence saturation have been proposed. As a result of this ambiguity, it is difficult to find a solution to prevent saturation. In this thesis, we further investigate a proposed mechanism behind quantum-cutting and luminescence saturation in Yb^{3+}-doped perovskites. We measured a temperature dependence of the NIR-emission intensity in $CsPbCl_3$:Yb^{3+} nanocrystals that is qualitatively in line with a mechanism without a proposed intermediate trap state in the quantum cutting mechanism. This is in contrast to the measured temperature dependent saturation, which qualitative is in line with a mechanism with an intermediate trap state. Time dependent measurements showed no overshoot in the luminescence intensity during the first few milliseconds after inset of excitation, which should be visible if quantum cutting occurs through the proposed quantum cutting mechanism that involves dopant pairs.

KEYWORDS: *Quantum-cutting, Luminescence Saturation, Perovskite Nanocrystals*

■ INTRODUCTION

With the increasing global energy demand alongside the requirement of green energy production to prevent further global warming, increasing efforts are made in the development and implementation of photovoltaic systems.[1] Solar panels commonly make use of semiconductor materials capable of absorbing sunlight to convert it to electrical energy. The solar spectrum comprises a wide range of wavelengths, but conventional solar cells are optimised to convert photons with a specific wavelength that matches their bandgap.[2] As a result, sub-bandgap photons are transmitted, whereas supra-bandgap photons are inefficiently converted as their excess energy is lost as heat. The loss in efficiency due to this spectral mismatch can be addressed by utilising additional phosphors.

One strategy is to use quantum-cutting phosphors, which split high-energy photons into multiple low-energy photons that can be converted more efficiently.[2] $CsPbCl_3$ doped with ytterbium is a recently discovered quantum-cutting phosphor,[3,4] which converts blue and ultraviolet photons into two near-infrared (NIR) photons. Conventional silicon solar cells can absorb these NIR photons, thus doubling the energy gain of supra-bandgap photons (see figure 1). Previously investigated quantum-cutting phosphors are often not capable of strongly absorbing the high energy photons over a large spectral range while also converting the photons with high efficiency.[2] $CsPbCl_3:Yb^{3+}$ is a novel material that uniquely has both characteristics and therefore makes it desirable for application.[5]

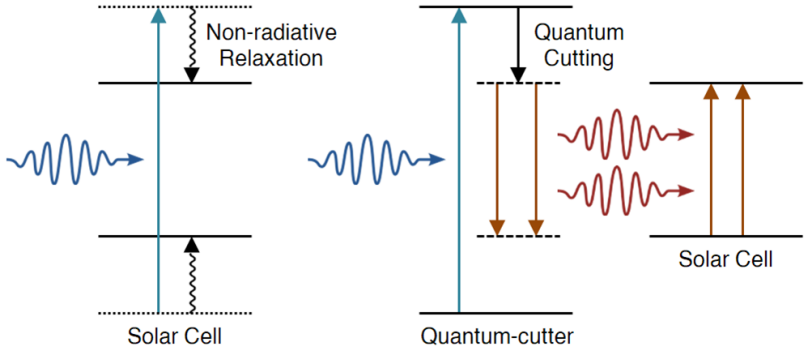

Figure 1 | Schematic figure showing the difference between a semiconductor solar cell without and with a quantum-cutting material. Excess energy of supra-bandgap photons gets lost as heat. Next-generation solar cells can be more efficient through addition of a quantum-cutting layer, which splits high-energy photons into multiple lower-energy photons that can all be efficiently converted.

A common problem of phosphors is luminescence saturation: the efficiency of converting light decreases as the intensity of incident light increases.[6] If the phosphor absorbs a photon shortly while still being in its excited state by a previous absorption event, the energy of the second photon can be lost as heat (see figure 2). Luminescence saturation in $CsPbCl_3:Yb^{3+}$ causes the quantum-cutting efficiency to drop significantly at light intensities comparable to normal daylight conditions.[7]

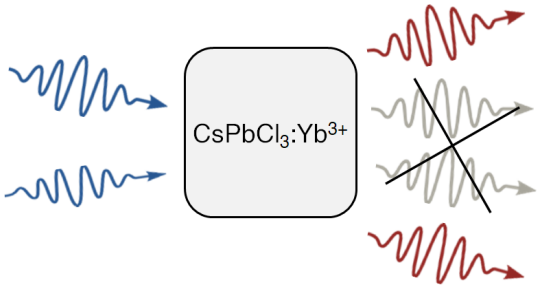

Figure 2 | Schematic figure showing how absorption of two photons within a short time-frame in $CsPbCl_3:Yb^{3+}$ does not lead to two quantum-cutting events due to luminescence saturation of the phosphor.

To find a solution to prevent this saturation, it is essential to understand both the mechanism behind quantum-cutting as well as its saturation. Substantial fundamental research on $CsPbCl_3$:Yb^{3+} nanocrystals (NCs) by the research group of Gamelin has given some insight into these mechanisms.[5,7–11] Due to the nature of doping, it is hypothesised that every two Yb^{3+}-dopants result in the formation of a Pb^{2+} vacancy for charge compensation.[5] This vacancy would introduce a highly efficient trap for the exciton to relax to within a picosecond timescale, lying below the conduction band edge. In addition to suppressing the excitonic emission, the trap state would cause efficient cooperative ET to two Yb-ions in neighbouring unit cells (Yb^{3+}-V_{Pb}-Yb^{3+}, a structure similar to *McPherson-pairs*)[12], because of high spatial overlap of the trapped exciton wavefunction with the dopants and similar transition energies. The formation of these pairs are supported by computational studies, showing that the formation energy of linear and right angle pairs of different lanthanides including ytterbium is negative and, so that these pairs can form spontaneously.[13]

Two different mechanism have been proposed for quantum cutting. The Song research group suggested that quantum cutting occurs through two consecutive steps.[3,4,14] The exciton would firstly relax to a deep trap state concomitant with excitation of an ytterbium dopant, and then relax to the ground state through a second excitation of an ytterbium dopant. The involvement of a deep trap state was suggested through the observation of trap luminescence. The Weiss research group suggested that quantum cutting occurs through reduction of a trivalent ytterbium dopant to its divalent state through electron transfer, followed by oxidation back to its trivalent state through hole transfer.[15] The hole transfer would be concomitant with quantum cutting, generating two ytterbium atoms in their excited state that are part of pairs, similar to the proposal of Gamelin. Figure 3 gives a schematic overview of the three different mechanisms proposed for quantum cutting.

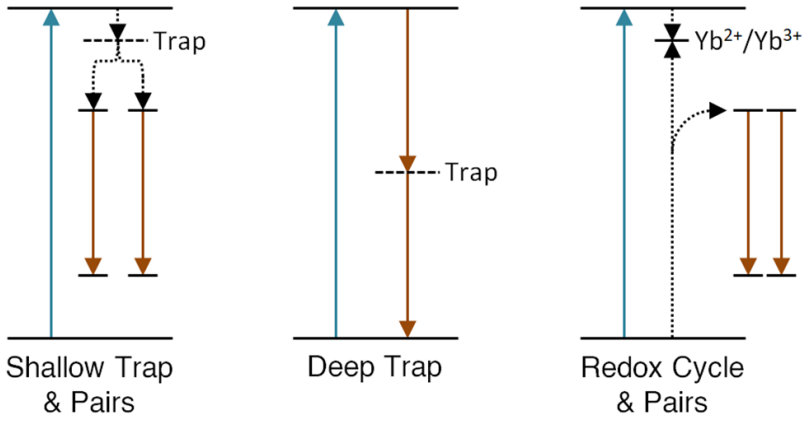

Figure 3 | Schematic figure showing the three different mechanisms proposed for the quantum cutting properties of $CsPbCl_3$:Yb^{3+}. From left to right, the mechanisms proposed by the research group of Gamelin,[5] Song[3] and Weiss[15].

In this thesis, we investigate the temperature dependence of the steady-state NIR-luminescence intensity at low incident light intensity as well as the temperature dependence of the NIR-luminescence saturation in $CsPbCl_3$:Yb^{3+} NCs. The temperature dependent NIR-luminescence intensity follows behaviour that is qualitatively similar to what a theoretical model predicts which excludes a trap state. This is in contrast to the measured temperature dependence of luminescence saturation, which is qualitatively more in line with the prediction of a theoretical model that includes a trap state. A model in which quantum cutting occurs through pairs predicts a decrease in the quantum cutting rate as a steady-state is reached after inset of excitation. This would result in an overshoot in the luminescence intensity in the first few milliseconds after inset of excitation. We measure the time-dependent NIR-emission in $CsPbCl_3$:Yb^{3+} NCs at high excitation rates but do not observe an overshoot, thus finding no supporting evidence for the involvement of pairs in the quantum cutting mechanism.

We start by discussing the quantum-cutting and luminescence saturation model proposed by the research group of Gamelin. We then discuss the difference between their proposed mechanism and their model, and build towards a model that firstly incorporates the proposed trap state and later on also the proposed involvement of pairs. We test

the mechanism that includes a trap state through measuring the temperature dependent NIR-intensity, as well as the saturation, by comparing it to modelled predictions. We then test the involvement of pairs in quantum-cutting through time-dependent measurements. Lastly, we discuss the possibility of luminescence saturation occurring through a mechanism involving divalent ytterbium dopants, which the research group of Weiss recently proposed to be part of the quantum-cutting process.

■ Theory

Semiconductors[16]

Semiconductors form a class of materials characterised by a bandgap, which is a range of energies which can not be occupied with electrons. The highest occupied state is then often referred to as the highest occupied molecular orbital (HOMO), and the lowest unoccupied state as the lowest occupied molecular orbital (LUMO). They respectively reside at the top and bottom of bands of states, called the valence band (VB) and conduction band (CB). Electrons in the semiconductor can be excited from the valence band to the conduction band by absorption of a photon with energy equal or greater than the bandgap. Because these transitions are allowed, the absorption cross sections of semiconductors are high. As a result, semiconductors are good absorbers of light over a wide spectral range. The absence of an electron in the valence band can be described as a positive quasi-particle referred to as a hole. Through the Coulomb force, the negatively charged electron in the conduction band and the positively charged hole are attracted to each other and can form an electron-hole pair which is called an exciton. The exciton can recombine through different ways. If the exciton has energy greater than the bandgap, this excess energy is quickly lost through relaxation to the bandedges. The exciton can then relax either radiatively, in which case a photon is emitted with energy equal to the bandgap, or non-radiatively, in which case the energy is lost through heat. The charge carriers can also get trapped on states that are formed through defects or surface states. These defects often lead to non-radiative decay of the exciton, but can sometimes lead to radiative decay, accompanied with emission of sub-bandgap photons. Emission from these defects, which are often referred to as traps, is called trap emission. If the traps are within the bandgap but close to a bandedge, they are called shallow traps, contrary to deep traps.

Lanthanides

The lanthanides form a series of 15 elements (atomic number 57-71) through which the seven 4f-orbitals are filled with electrons, generally symbolised by Ln.[17] They are often most stable in their trivalent oxidation state, and as a result of their large ionic radii, lanthanides can often only be doped in crystals in which they can occupy sites with a coordination number of six or higher and replace ions of the host crystal with the same charge (isovalent doping). The Pb-site in $CsPbCl_3$ has an octrahedral environment,[18,19] thus providing suitable host for the lanthanides. The lead atom is in its divalent state however, an example of uncommon aliovalent doping. If the 4f-orbitals are only partially filled, which is the case for all lanthanides except lanthanum and lutetium, there are different configurations of filling the orbitals possible. As a result of coloumbic interaction between the 4f-electrons, different configurations of filled 4f-orbitals have different energies associated with them.[20] Spin-orbit coupling results in further splitting of the energies of different configurations. Lastly, the environment of the lanthanide also affects the energies of different configurations through an effect called crystal field splitting. The effect is dependent on the crystal lattice of the host, but is weak as the 4f-orbitals are screened by the 5s- and 5p-orbitals. The lanthanides can be excited from their ground state configuration to an excitation state configuration by absorption of a photon. The absorption cross section of lanthanides is low as f-f transitions are forbidden.[17] The lanthanides can then relax to the ground state through emission of a photon. Because the f-orbitals are shielded from the environment, there is weak coupling between molecular vibrations and the electronic transitions, which results in narrow absorption and emission bands.[17,20] The narrow absorption bands in combination with their low absorption cross section makes lanthanides poor absorbers.

■ METHODS

Chemicals

Chemicals used include cesium acetate (99.9%, Sigma-Aldrich), hexane (97%, Honeywell), oleic acid (90%, Sigma-Aldrich), oleylamine (80-90%, Sigma-Aldrich), 1-octadecene (90%, Sigma-Aldrich), ethyl acetate (99.5%, Honeywell), lead acetate trihydrate (99.99%, Sigma-Aldrich), trimethylsilyl chloride (99%, Sigma-Aldrich), ytterbium acetate tetrahydrate (99.9%, Sigma-Aldrich). All chemicals were used without further purification unless specified otherwise.

Synthesis of $CsPbCl_3$:Yb^{3+} NCs

0.8 mmol cesium acetate, 0.1 mmol lead acetate trihydrate, 0-0.2 mmol ytterbium acetate tetrahydrate (0-7 Yb^{3+}%), 10 ml 1-octadecene, 2 ml oleic acid and 0.5 ml oleylamine were added to a 25 ml three-necked-round-bottom-flask in a heating mantle. The solution was degassed at room temperature for 10 min. and kept under vacuum for 1 h at 110 °C. The temperature was then raised to 240 °C at which point 0.4 ml trimethylsilyl chloride was injected after which the heating element was immediately replaced by a water bath. After the solution cooled down to room temperature, it was centrifuged at 6000 RCF for 5 min. The residue was then redissolved in 5 ml hexane and 5 ml ethyl acetate and centrifuged at 6000 RCF for 5 min. The product was then redissolved in 5 ml hexane.

Temperature Dependent Emission and Luminescence Saturation Measurements

A 375 nm laser (Coherent OBIS) was used to excite dried samples of $CsPbCl_3$:Yb^{3+} NCs. The power of incident light was varied by varying the laser power in addition to using reflective neutral density filters (Thorlabs). A 90/10 plate beamsplitter (Thorlabs) in addition to a power meter (Thorlabs PM130D) was used to record the intensity of incident light for every measurement. The fluence was calculated by using the beam diameter of the collimated laser beam reported by the supplier (0.7 mm). A 900 nm LP filter (Thorlabs) was placed in the emission path and the emission spectra were recorded with a spectroscope (Andor Kymera 193i) equipped with a 600 l/mm grating blazed at 1000 nm. Temperatures were varied using a liquid nitrogen in addition to a heating element in a optical cryostat (Oxford Instruments).

Square-pulse Excitation Profile Measurements

$CsPbCl_3$:Yb^{3+} (<0.1%) NCs were spin-coated on 1 mm microscope slide (Menzel Gläser) with a coverslip (Menzel Gläser). On a Microscope (Nikon Eclips Ti-U), the samples were excited at varying incident powers using a 375 nm laser (Coherent OBIS) in addition to reflective neutral density filters (Thorlabs). The laser was modulated by a laser driver (Picoquant PDL 800D) with a pulse length of 10 ms at a frequency of 20 Hz. The sample was excited in focus using an oil-immersion objective (Nikon CFI Plan Apochromat Lambda 100x, NA 1.45) through which also the NIR-luminescence was collected by making use of a dichroic mirror. The light passed through a 900 nm LP filter (Thorlabs) and IR fiber optic cable (Thorlabs, P1-780A-FC-1), and was recorded using a superconducting nanowire single-photon detector (SNSPD) system (Single Quantum EOS). A time-to-digital converter (qutools quTAG) was connected to the SNSPD to obtain information about the laser-pulse and photon-detection events.

Monte Carlo Simulations

A list of positions of lead atoms in a cubic $CsPbCl_3$ NC with edge length 11 nm was created (a = 5.6 Å)[21]. Iteratively, a random vacancy was replaced by a lead atom and two random lead atoms of neighbouring unit cells were replaced by ytterbium atoms, until the dopant concentration was reached. The distances between all ytterbium atoms were calculated and used to calculate the average migration rate using $C_M = 2.36 \cdot 10^9$ Å^6 s^{-1} (see main text for derivation).

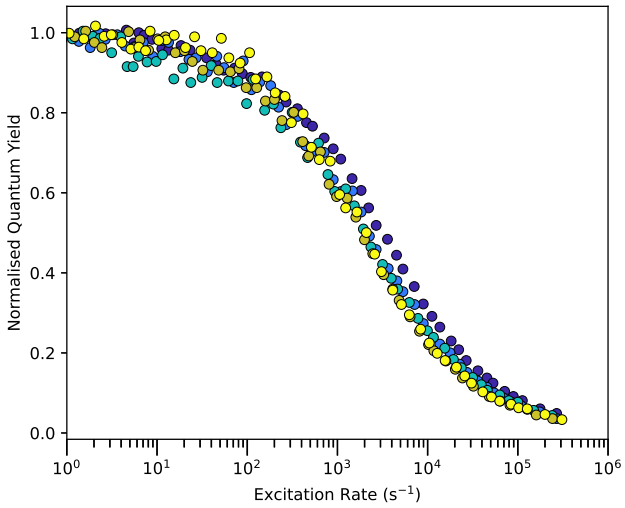

Figure 4 | Semilog plot of the normalised NIR-QY against excitation rate for CsPb($Cl_{1-x}Br_x$)$_3$:Yb^{3+} NCs with x ranging from 0 to 0.75 (purple to yellow). Reproduced from Erickson et al.[7]

■ RESULTS AND DISCUSSION

Gamelins Saturation Model

The Gamelin research group previously investigated the effect of the excitation rate on the NIR-QY of $CsPbCl_3$:Yb^{3+} NCs and observed they are prone to luminescence saturation under normal solar irradiance, as shown in figure 4.[7] To explain the luminescence saturation, a model was proposed that fits well to the data. This model includes the possibility of an Auger-type cross-relaxation process in which the energy of a photo-excited nanocrystal is transferred to an Yb^{3+} in its $^2F_{5/2}$ excited state to create a highly excited Yb^{3+} dopant, which can then relax back to its luminescent state via internal conversion and phonon emission. We discuss their model to gain insight on the dependence of the quantum yield on the doping concentration and size of the system.

Their model consist of two differential equations, that describe the effect of various processes on the populations of excitons (N_1) and excited ytterbium dopants (n_{Yb_1}): photo-excitation of the nanocrystal, quantum cutting, radiative decay of the exciton and ytterbium dopants and two different Auger processes (AP). The ground state populations are denoted with the subscript 0. With no incident light, the ground state population of excitons is equal to the degeneracy of the exciton energy level, which was assumed to be one for nanocrystals, and the ground state population of ytterbium dopants is equal to the total number of dopants. The average total number of dopants can be calculated with the dopant concentration, nanocrystal size and unit cell size. In addition to modelling an Auger process in which the energy of the exciton is transferred to an excited ytterbium dopant (AP_1), similar to the Gamelin research group, we also investigate the reverse process in which an excited ytterbium dopant transfers its energy to an exciton, generating a hot exciton (AP_2). Their model describing luminescence saturation in $CsPbCl_3$:Yb^{3+} NCs then looks like the following:

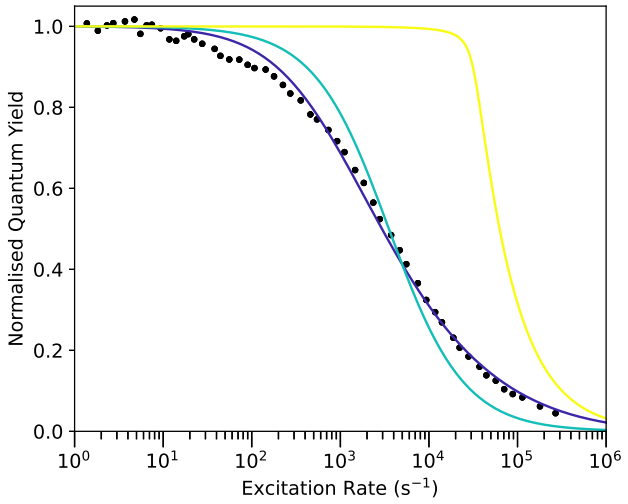

Figure 5 | Semilog plot of the normalised NIR-QY against excitation rate in $CsPbCl_3$:Yb^{3+} (1.4%) predicted by best fits of Gamelins model (AP_1 and AP_2, purple and green respectively) compared with their data (black) along with the saturation predicted for only ground state depletion of Yb^{3+} (yellow).

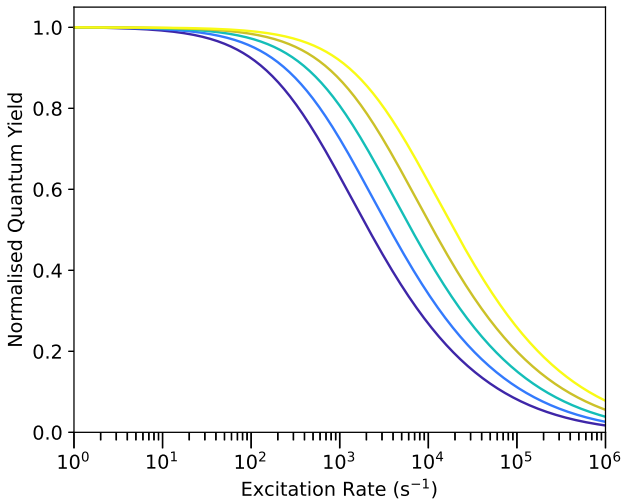

Figure 6 | Semilog plot of the normalised NIR-QY against excitation rate in $CsPbCl_3$:Yb^{3+} predicted Gamelins model (AP_1) for varying ytterbium concentrations indicated by colour ranging logarithmically from 1% to 10% (purple to yellow).

Gamelins Saturation Model

$$\frac{dN_1}{dt} = \underbrace{k_E N_0}_{\substack{\text{Nanocrystal}\\ \text{Excitation}}} - \underbrace{k_{QC}\frac{n_{Yb_0}}{2}N_1}_{\substack{\text{Quantum}\\ \text{Cutting}}} - \underbrace{k_{EL}N_1}_{\substack{\text{Radiative}\\ \text{Decay}\\ \text{(Exciton)}}} - \underbrace{k_{AP_1}n_{Yb_1}N_1}_{\substack{\text{Auger Process}\\ \text{Type 1}}} \tag{1.1}$$

$$\frac{dn_{Yb_1}}{dt} = \underbrace{k_{QC}N_1 n_{Yb_0}}_{\substack{\text{Quantum}\\ \text{Cutting}}} - \underbrace{k_{Yb}n_{Yb_1}}_{\substack{\text{Radiative}\\ \text{Decay}\\ \text{(Ytterbium)}}} - \underbrace{k_{AP_2}n_{Yb_1}N_1}_{\substack{\text{Auger Process}\\ \text{Type 2}}} \tag{1.2}$$

Solving this system of differential equations under steady-state conditions, in which the populations do not change over time, can be done analytically. This gives two equations that describe the populations of excitons and excited state ytterbium atoms. The NIR-QY can then be calculated as a function of the excitation rate and the population of Yb ions in the excited state:

$$\mathrm{QY} = \frac{k_{Yb}n_{Yb_1}}{k_E} \tag{2}$$

This model is able to predict the quantum yield as a function of excitation rate well for a mechanism involving AP_1, as shown in figure 5 in which it is compared to experimental data of Gamelins research group, but not for a mechanism involving AP_2. We also included the saturation in case of only ground state depletion of Yb^{3+} (yellow line). This predicts a quantum yield that does not decrease until the excitation rate approaches the maximum emission rate ($n_{Yb}k_{Yb}$). Clearly ground state depletion, in which the quantum-cutting rate is limited through the depletion of ytterbium atoms in the ground state, can not explain the observed saturation. We will now analyse how the degree of saturation depends on the doping concentration and size of the nanocrystal.

Equation 6 in combination with the solution for the steady-state population of excited ytterbium dopants can be used to derive an expression for the excitation rate that corresponds to obtain a certain quantum yield:

$$k_E(\mathrm{QY}) = \frac{k_{Yb}\left[\left(1+\frac{1}{2}\mathrm{QY}\right)k_{QC}n_{Yb} + \mathrm{QY}k_{EL}\right]}{\left(k_{AP_1} - \frac{1}{2}k_{QC}\right)\mathrm{QY}^2 + \left(k_{Yb}+k_{QC}\right)\mathrm{QY}} \tag{3}$$

Equation 3 predicts that the excitation corresponding to a certain quantum yield is linearly dependent on the number of ytterbium dopants. This is in contrast with the results of Gamelins research group, which found a non-linear relationship for their model.[7] Figure 3 shows how the predicted saturation curves shift linearly with dopant concentration. We can simplify equation 3 as the concentration independent term is negligible even at low dopant concentrations ($\mathrm{QY}k_{\mathrm{EL}} \ll \left(1+\frac{1}{2}\mathrm{QY}\right)k_{\mathrm{QC}}n_{\mathrm{Yb}}$):

$$k_{\mathrm{E}}(\mathrm{QY}) = \frac{\left(1+\frac{1}{2}\mathrm{QY}\right)k_{\mathrm{Yb}}k_{\mathrm{QC}}n_{\mathrm{Yb}}}{\left(k_{\mathrm{AP}_1}-\frac{1}{2}k_{\mathrm{QC}}\right)\mathrm{QY}^2+\left(k_{\mathrm{Yb}}+k_{\mathrm{QC}}\right)\mathrm{QY}} \tag{4}$$

As both the excitation rate and number of ytterbium dopants scale linearly with the volume of the NCs, equation 5 indicates the saturation is independent of the size of the NCs, such that only the dopant concentration needs to be considered for modelling and size polydispersity can be ignored. In addition, because the excitation rate, at which a certain NIR-QY is reached, is linearly dependent on the number of ytterbium dopants, the excitation rate that matters is the excitation rate per ytterbium dopant:

$$\frac{k_{\mathrm{E}}}{n_{\mathrm{Yb}}}(\mathrm{QY}) = \frac{\left(1+\frac{1}{2}\mathrm{QY}\right)k_{\mathrm{Yb}}k_{\mathrm{QC}}}{\left(k_{\mathrm{AP}_1}-\frac{1}{2}k_{\mathrm{QC}}\right)\mathrm{QY}^2+\left(k_{\mathrm{Yb}}+k_{\mathrm{QC}}\right)\mathrm{QY}} \tag{5}$$

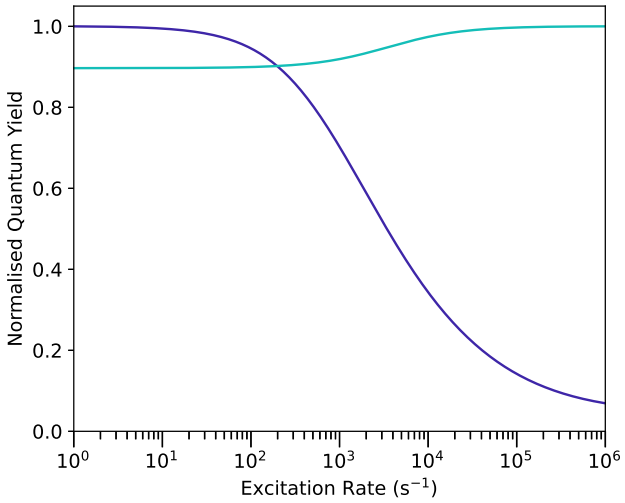

Figure 7 | Semilog plot of the normalised exciton QY against excitation rate in $CsPbCl_3$:Yb^{3+} (1.4%) predicted by Gamelins model (AP_1 and AP_2, purple and blue respectively).

Similar to the NIR-QY, the QY of the exciton can also be predicted through the model:

$$\mathrm{QY} = \frac{k_{\mathrm{EL}}N_1}{k_{\mathrm{E}}} \tag{6}$$

Figure 7 shows the quantum yield as a function of the excitation rate of the exciton luminescence predicted by Gamelins model for for a mechanism involving AP_1 and AP_2 (purple and blue respectively). For for a mechanism involving AP_1, in which the energy of the exciton is transferred to an excited ytterbium dopant, it follows similar behaviour to the saturation of the NIR-QY. As the excitation rate increases, the steady-state population of ytterbium dopants increases, concomitant with an increase in rate of the Auger process. The Auger process is in competition with radiative decay of an exciton, such that the probability at which an exciton decays radiatively decreases with increasing excitation rate, explaining the predicted saturation of the exciton luminescence. For for a mechanism involving AP_2, in which the energy of the excited ytterbium dopant is transferred to an exciton, the quantum yield is predicted to stay quite constant, with a small increase above $\sim 10^3$ s^{-1}. As the excitation rate increases, the steady-state population of excited ytterbium dopants increases, concomitant with a decrease of the quantum-cutting rate. Therefore, as quantum-cutting is in competition with radiative

decay of the exciton, the probability at which the exciton relaxes radiatively increases as the excitation rate increases. This explains the inverse-saturation, the increase of the quantum-cutting rate with excitation rate, of the exciton luminescence.

Both models predict a non-linear increase of the exciton luminescence with the excitation rate. Despite these predictions, the exciton luminescence has been measured in $CsPbCl_3$:Yb^{3+} NCs to increase linearly with the excitation rate.[7] The highest used excitation rate for these measurements was only $2 \cdot 10^4$ s^{-1}. However, non-linear behaviour in the exciton quantum yield as a function of the excitation rate as a result of luminescence saturation is predicted to occur above $\sim 10^3$ s^{-1} for AP_2 at a dopant concentration of 1.4%, at which only a few measurements were done. Additionally, the change in quantum yield is predicted to be ~ 10%, such that with few data points with a high uncertainty, the non-linear behaviour can remain unnoticed. The expected behaviour of the quantum yield of the exciton as a function of the excitation rate has not been described earlier. As we have shown here, it can also provide insight in the mechanism behind saturation.

To conclude, the saturation of the NIR-QY can be described well by a model in which the energy of the exciton is non-radiatively lost through energy transfer to a ready excited ytterbium dopant, but the model is in disagreement with the measured exciton quantum yield as function of excitation rate. Additional measurements for the exciton quantum yield as a function of excitation rate at higher powers are required to further test the proposed models.

Including Trapping and Fixed Pairs

Based on transient absorption measurements and the measurement of emission with energy slightly lower of the exciton, the Gamelins research group proposed the presence of a shallow trap state to which the exciton relaxes within a picosecond time frame, from which quantum-cutting occurs. We will refer to such a trapped exciton as a bound exciton, in line with the description used for similar observed shallow luminescent trap states in caesium lead halide NCs and SCs.[19,22–24] Their model for luminescence saturation neglects this intermediate trap state. The quantum-cutting is described by a single process involving the cooperative energy transfer (CET) from the exciton state to two ytterbium atoms.[7] Additionally, by neglecting the trap state, the proposed pair structures responsible for quantum-cutting are implied but not explicitly modelled (implicit pairs); The exciton can transfer its energy to any combination of two ytterbium dopants in the ground state. We will refer to this as quantum-cutting through random pairs.

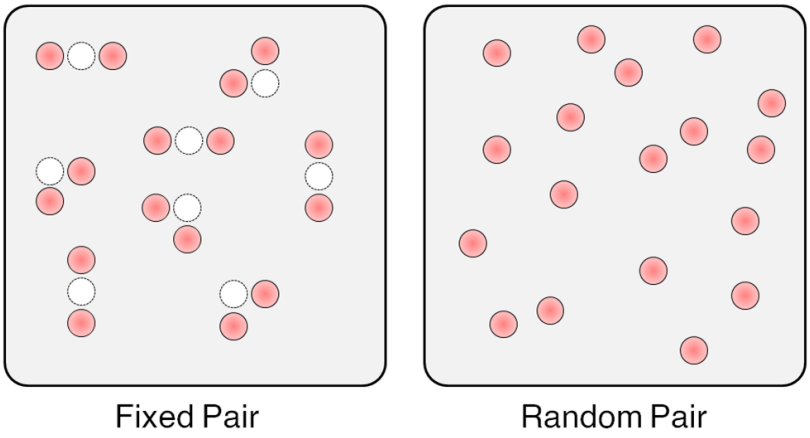

Figure 8 | Schematic depiction of quantum-cutting occurring through pair structures, which we refer to as quantum-cutting through fixed pairs, and through any combination of two ytterbium dopants, which we refer to as quantum-cutting through random pairs.

We extend their model by sequentially adding both proposed processes: trapping, within picoseconds,[5,25] followed by CET, within nanoseconds (see figure 9). Additionally, we explicitly model the involvement of pair structures in the quantum-cutting process (fixed pairwise quantum-cutting). This tests if the predicted saturation is still in line with the measurement.

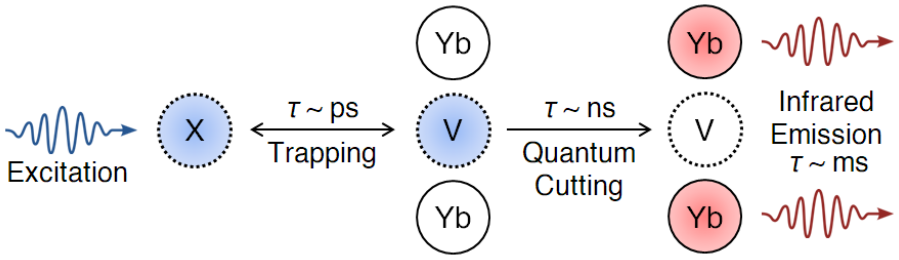

Figure 9 | Schematic depiction of the quantum-cutting mechanism proposed by the Gamelin research group. Following excitation, the exciton (X) quickly gets trapped on a charge-compensating vacancy (V). Sequentially, Ytterbium atoms (Yb) in neighbouring unit cells can efficiently be excited through a single quantum-cutting step.

If trapping indeed occurs within picoseconds, then it is reasonable to neglect this process in the model and treat the quantum-cutting as though it does not involve the trap state, as the rate limiting step for quantum-cutting is CET. Additionally, if the Auger process occurs by ET from the exciton to an excited ytterbium dopant, the trap state is not needed to be considered in the model. However, similar to how the CET is proposed to occur from the trap state, the Auger process could also occur by ET from the trap state. The Auger rate is then no longer simply dependent on the product of the number of free excitons and excited ytterbium dopants. To investigate this possibility, a model that considers

the trap state is required. As we will also show, the predicted behaviour of the temperature dependent NIR-luminescence intensity and saturation are significantly different when taking the trap state into account.

Trap Luminescence

Trap luminescence (TL), an additional emission peak at energy slightly below that of the exciton, has been observed in $CsPbCl_3:Ln^{3+}$ ($Ln^{3+} = La^{3+}, Yb^{3+}$) NCs,[5,19,25] This has not been observed in undoped NCs, which lead to the conclusion that trivalent dopants would introduce these trap states.[5] We will show that the measured NIR quantum yield at low temperatures is not in line with the theoretically expected value when trap luminescence originates from the same trap state proposed to be part of the quantum-cutting mechanism. This allows us to neglect trap luminescence from the model for luminescence saturation.

At a cryogenic temperature, the trap luminescence in $CsPbCl_3:La^{3+}$ NCs was measured to have a high decay rate, with a lifetime in the order of tens of picoseconds. Combined with the high NIR-QY of $CsPbCl_3:Yb^{3+}$ NCs, it was concluded the quantum-cutting rate must be even faster than trap luminescence, on the picosecond timescale.[5] If trap luminescence and quantum-cutting occur from the same energy state as has been proposed,[5] the expected NIR-QY at low excitation power can be approximated by:

$$\mathrm{QY} = \frac{2k_{\mathrm{CET}}}{k_{\mathrm{TL}}} \tag{7}$$

However, more recent work showed that the rise time of luminescence from ytterbium, attributed to the quantum-cutting rate, is in the order of tens of nanoseconds.[18] The orders of magnitude higher decay rate of trap luminescence than the quantum-cutting rate despite a NIR-QY approaching 2 suggests that either the trap luminescence is of significantly slower nature in $CsPbCl_3:Yb^{3+}$ than $CsPbCl_3:La^{3+}$, or that the quantum-cutting and trap luminescence are not in direct competition by not originating from the same energy state. The NIR-QY decreases with decreasing temperature as both the quantum-cutting rate and the radiative decay rate of ytterbium decrease, while the competitive exciton decay rate increases with decreasing temperature. With the highest reported NIR-QY of $\sim$190% at room temperature[8] and the temperature dependence of the NIR-emission intensity ($I_{15K}/I_{293K} = 0.57$)[18], the NIR-QY can be $\sim$100% at most at 15 K. From equation 7, we then calculate that the lifetime of trap luminescence in $CsPbCl_3:Yb^{3+}$ must be in the order of microseconds at cryogenic temperatures, 5 orders of magnitude slower than that measured in $CsPbCl_3:La^{3+}$. Given the similarity in chemical properties of lanthanum and ytterbium, such a large difference in the decay rate of trap states is unlikely, from which we conclude the trap luminescence must originate from a different energy state than quantum-cutting. We therefore exclude trap luminescence from the model for luminescence saturation.

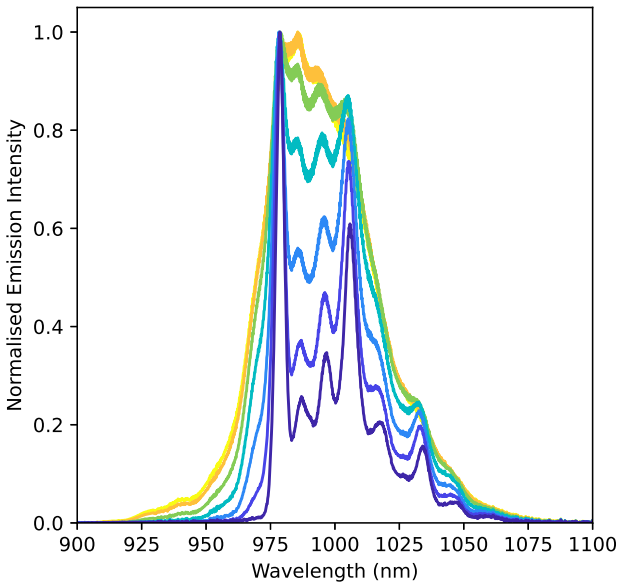

Figure 10 | Normalised NIR-luminescence spectra measured at $9.4, 51.4, 98.9, 150.3, 200.9, 252.1, 293.1$ K (purple to yellow) of $CsPbCl_3:Yb^{3+}$ excited with a 375 nm laser.

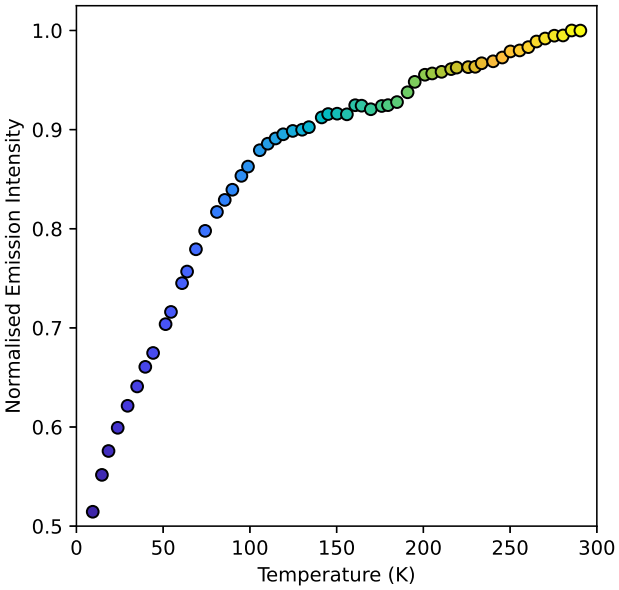

Figure 11 | Measured integrated NIR-luminescence intensity normalised by the intensity measured at room temperature of $CsPbCl_3:Yb^{3+}$ excited with a 375 nm laser. Colors correspond to spectra of figure 10.

Temperature Dependent NIR-Luminescence Intensity

The rate of trapping and detrapping are temperature dependent due to possibility to overcome the energetic barriers through absorption of one or multiple phonons. Phonons can be described as collective vibrations of atoms in a crystal associated with a quantised amount of energy. The energy of the most energetic phonon is dependent on the crystal and temperature, and is ~ 30 meV (~ 1.2 kT at room temperature) for $CsPbCl_3$ at room temperature.[26] The activation barrier for trapping is unknown and, with our conclusion that trap luminescence and quantum-cutting must originate from different energy states, so is the energy difference between the free and bound exciton state. By incorporating the trap state in the model, we can calculate the expected steady-state NIR-QY as function of the temperature, activation barrier, and energy difference between the free and bound exciton. We therefore create an extended model that includes an intermediate trap state and is temperature dependent. By comparing the measured change in NIR-intensity with that predicted by the model, we can gain information about the depth of the trap state and the height of the activation barrier.

Figure 10 shows the measured temperature dependent normalised NIR-emission spectra. At room temperature, a broad emission band centered around 990 nm is visible. At cryogenic temperature, several sharp emission peaks are distinguishable, with the most prominent centered around $979, 987, 997, 1006, 1017, 1034$ nm. The ratio between the emission intensity of different peaks is also strongly temperature dependent, with for example the peak at ~ 979 nm becoming increasingly prevalent at lower temperatures. These results are in line with previously reported results.[18] the Gamelin research group suggested that the different peaks in the spectrum are a result of different ytterbium species due to the possibility of different charge-compensation motifs with differing NIR-emission. The difference in the emission spectra at different temperatures can then be explained through a difference in the temperature dependence of the quantum-cutting or energy transfer rates of different ytterbium species.

Figure 11 shows the measured temperature dependent NIR-luminescence intensity normalised by the NIR-luminescence intensity at 293 K under low excitation rates. The NIR-luminescence appears to lower approximately linearly with decreasing temperature and experiences a sharper decrease at temperatures below ~ 110 K. To investigate the effect of temperature on the predicted NIR-luminescence intensity and saturation as a result of incorporating the trap state in the model, the temperature dependence of the trapping and detrapping rate are required. The rate of trapping and detrapping

(k_{T} and k_{D} respectively) can be described by the following equations:[23,24]

Thermally Assisted Trapping Model

$$k_{\mathrm{T}}(T) = k_{\mathrm{F}} T e^{-E_{\mathrm{A}}/k_{\mathrm{B}}T} \tag{8.1}$$

$$k_{\mathrm{D}}(T) = k_{\mathrm{F}} T e^{-(\Delta E + E_{\mathrm{A}})/k_{\mathrm{B}}T} \tag{8.2}$$

k_{F} is a temperature independent rate constant, T is the absolute temperature, E_{A} is the activation barrier for trapping, ΔE is the energy energy difference between the free and bound exciton state, and k_{B} is the Boltzmann constant. With an estimate for the trapping rate at room temperature, the temperature independent rate constant can be approximated. This in turn allows us to calculate the temperature dependent trapping and detrapping rates using this thermal-assisted trapping model. The model is schematically shown in figure 12.

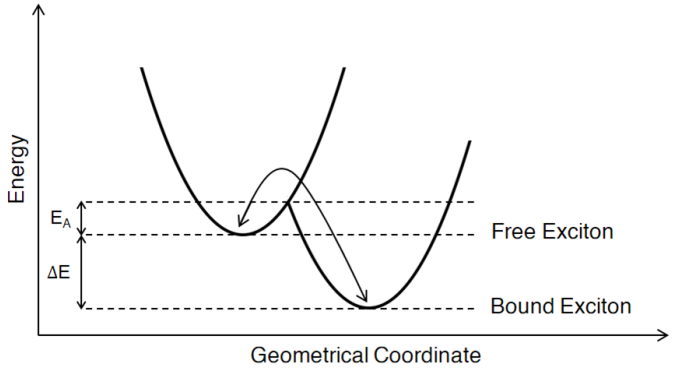

Figure 12 | Schematic depiction of trapping and detrapping processes between the free and bound exciton state, separated by an energy difference (ΔE) and accompanied with an activation energy (E_{A}).

We can then extend the model of Gamelin by including one additional differential equation to account for the population of bound excitons (V_1):

Extended Saturation Model

Trap State & Implicit Pairs

$$\frac{dN_1}{dt} = k_{\mathrm{E}} N_0 - k_{\mathrm{EL}} N_1 - k_{\mathrm{T}} V_0 N_1 + k_{\mathrm{D}} V_1 N_0 - k_{\mathrm{AP}} N_1 n_{\mathrm{Yb}_1} \tag{9.1}$$

$$\frac{dV_1}{dt} = k_{\mathrm{T}} V_0 N_1 - k_{\mathrm{D}} V_1 N_0 - k_{\mathrm{QC}} V_1 \left(\frac{n_{\mathrm{Yb}_0}}{n_{\mathrm{Yb}}}\right)^2 \tag{9.2}$$

$$\frac{dn_{\mathrm{Yb}_1}}{dt} = 2k_{\mathrm{QC}} V_1 \left(\frac{n_{\mathrm{Yb}_0}}{n_{\mathrm{Yb}}}\right)^2 - k_{\mathrm{Yb}} n_{\mathrm{Yb}_1} \tag{9.3}$$

At low excitation rates the Auger process can be neglected (i.e. saturation occurs to an insignificant degree). In addition, the ground state populations can be approximated by their degeneracy as an insignificant fraction is excited (N_0=1, V_0=$\frac{1}{2}n_{\mathrm{Yb}}$, n_{Yb_0}=n_{Yb}). These simplifications allow us to derive an analytical expression for the steady-state population of excited ytterbium dopants at low excitation rates, and combined with equation 6, an expression for the NIR-QY:

$$\mathrm{QY} = \left[\frac{k_{\mathrm{EL}}}{k_{\mathrm{T}} n_{\mathrm{Yb}}}\left(1 + \frac{k_{\mathrm{D}}}{k_{\mathrm{QC}}}\right) + \frac{1}{2}\right]^{-1} \tag{10}$$

Similarly, we derive an analytical expression for the NIR-QY at low excitation rates for the model without an intermediate trap state:

$$\mathrm{QY} = \left(\frac{k_{\mathrm{EL}}}{k_{\mathrm{QC}} n_{\mathrm{Yb}}} + \frac{1}{2} \right)^{-1} \tag{11}$$

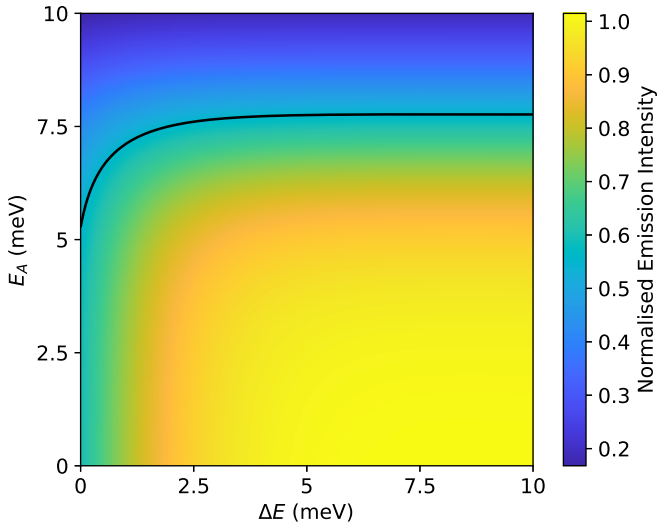

Figure 13 | NIR-luminescence intensity in $CsPbCl_3:Yb^{3+}$ (1.4%) NCs at 15 K normalised by the NIR-luminescence intensity at 293 K (I_{15K}/I_{293K}) as function of activation barrier and energy difference between the free and bound exciton predicted by equation 10. The black line illustrates the measured I_{15K}/I_{293K} of 0.55.

Figure 13 shows the NIR-luminescence intensity at 15 K normalised by the NIR-luminescence intensity at 293 K (I_{15K}/I_{293K}) as function of activation barrier and energy difference between the free and bound exciton. The black line illustrates the combinations of the activation energy and the energy difference between the free and bound exciton that predicts the measured I_{15K}/I_{293K} (0.55, in close agreement with an earlier reported value of 0.57)[18]. The temperature dependent rate constants for trapping and detrapping were respectively obtained via equation 8.1 and 8.2, and for quantum-cutting and exciton decay from earlier reported data.[18,27] It can be seen that at 15 K, the model predicts that the NIR-luminescence intensity is only a function of the activation barrier for trapping at a sufficiently high energy difference between the free and bound exciton state. The energy difference between the free and bound exciton state only affects the detrapping rate, such that at a sufficiently high energy difference ($\Delta E > \sim 5$ meV), quantum-cutting occurs much faster than detrapping at cryogenic temperatures. This is reflected in equation 10 by $k_{\mathrm{D}}/k_{\mathrm{QC}}$ becoming negligible with respect to one, in which case the equation can be simplified to:

$$\mathrm{QY} = \left(\frac{k_{\mathrm{EL}}}{k_{\mathrm{F}} T n_{\mathrm{Yb}}} e^{E_{\mathrm{A}}/k_{\mathrm{B}}T} + \frac{1}{2} \right)^{-1} \tag{12}$$

which is indeed only dependent on the activation barrier, not the energy difference between the free and bound exciton state.

With estimates for possible combinations of the activation barrier and the energy difference between the free and bound exciton state, we model the temperature dependent normalised NIR-luminescence intensity (I_T/I_{293K}) including and excluding the trap state, using equation 10 and 11 respectively. The result for the model without the trap state (figure 14) qualitatively matches the measured temperature dependent NIR-emission intensity (figure 11). The predicted decrease in NIR-emission intensity with decreasing temperature is the result of a decrease in the quantum-cutting rate and the decay

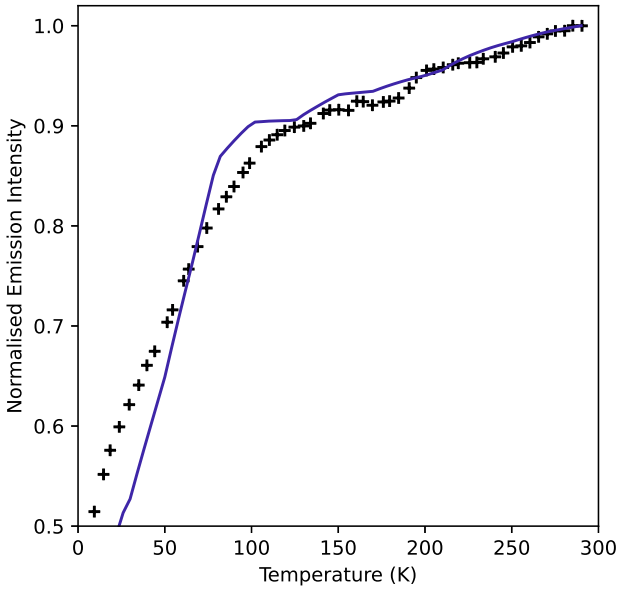

Figure 14 | Modelled and measured NIR-luminescence intensity normalised by the intensity measured at room temperature in $CsPbCl_3$:Yb^{3+} (1.4%) NCs for the model without an intermediate trap state.

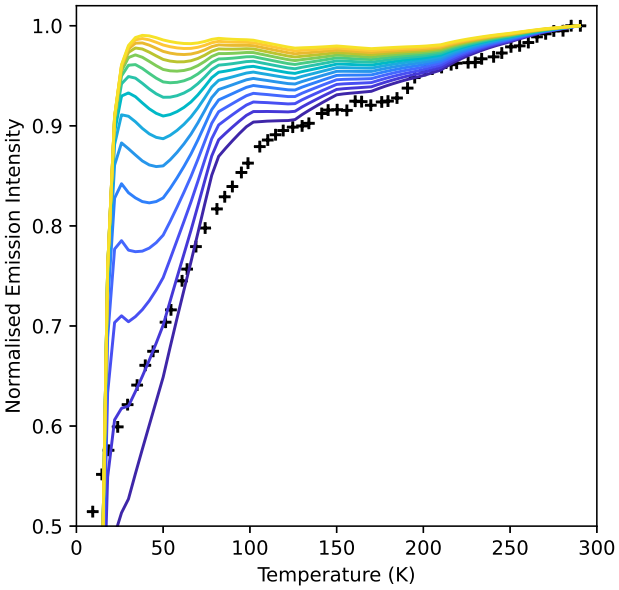

Figure 15 | Modelled NIR-luminescence intensity normalised by the intensity measured at room temperature in $CsPbCl_3$:Yb^{3+} (1.4%) NCs for the model with an intermediate trap state. The energy difference between the free and bound exciton state is increased linearly from 0 to 150 meV (purple to yellow).

rate of ytterbium, as well as an increase in the decay rate of the exciton. The intensity lowers with decreasing temperature and drops as the temperature falls below ~ 100 K, as the quantum-cutting rate decreases significantly. The result for the model with the trap state (figure 15) qualitatively matches the measured temperature dependent NIR-emission intensity only at an energy difference between the free and bound exciton close or equal to zero. As the energy difference increases, the predicted rate at which the intensity lowers with the temperature decreases and even becomes negative (intensity increases with lowering temperature) as it increases above ~ 50 meV. Intuitively, this behaviour can be explained by a decrease in the detrapping rate with increasing energy difference and decreasing temperature. This in turn leads to a higher quantum-cutting to exciton recombination ratio. To conclude, the temperature dependent NIR-luminescence supports the model for quantum-cutting without an intermediate trap state. A model for quantum-cutting with an intermediate trap state can explain the observed temperature dependent NIR-luminescence only if the trap state lies close (a few meV at most) below the free exciton state, at which point it would have little effect on the temperature dependent dynamics.

Model Including Pairwise Quantum-cutting

To include both the pairs and the trap states in the model, differential equations describing the population dynamics of pairs are required. A trap state can be filled or empty, and either none, one, or both of the neighbouring ytterbium dopants can be in its $^2F_{5/2}$ excited state, resulting in a total of 6 different energy states of pairs. Filled and empty trap states are denoted V_1 and V_0 respectively (V stands for vacancy), excited or ground state ytterbium dopants are denoted Yb_1 and Yb_0 respectively. Given the small expected energy difference between the excited state and the trap state thermally assisted detrapping is expected to occur significantly at room temperature. Thermally assisted detrapping has earlier been proposed for lanthanide doped $CsPbCl_3$ NCs.[28]

Due to the differentiation between the two exciton states, the Auger process of energy transfer to an excited ytterbium dopant can be modelled to either involve a bound or free exciton (AP_1 and AP_2 respectively). We also model the possibility of an Auger process involving energy transfer from an excited ytterbium dopant to an excited exciton state (AP_3). Figure 16 gives a schematic overview of these processes in a Jablonski diagram. Gamelins research group concluded this type of Auger process could not be responsible for the luminescence saturation based on results of their model. Internal conversion from the charge transfer state of ytterbium to its $^2F_{5/2}$ state is not considered in the model, as we assume similar to the assumption made by Gamelins group,[7] that this relaxation is sufficiently fast such that it can be neglected.

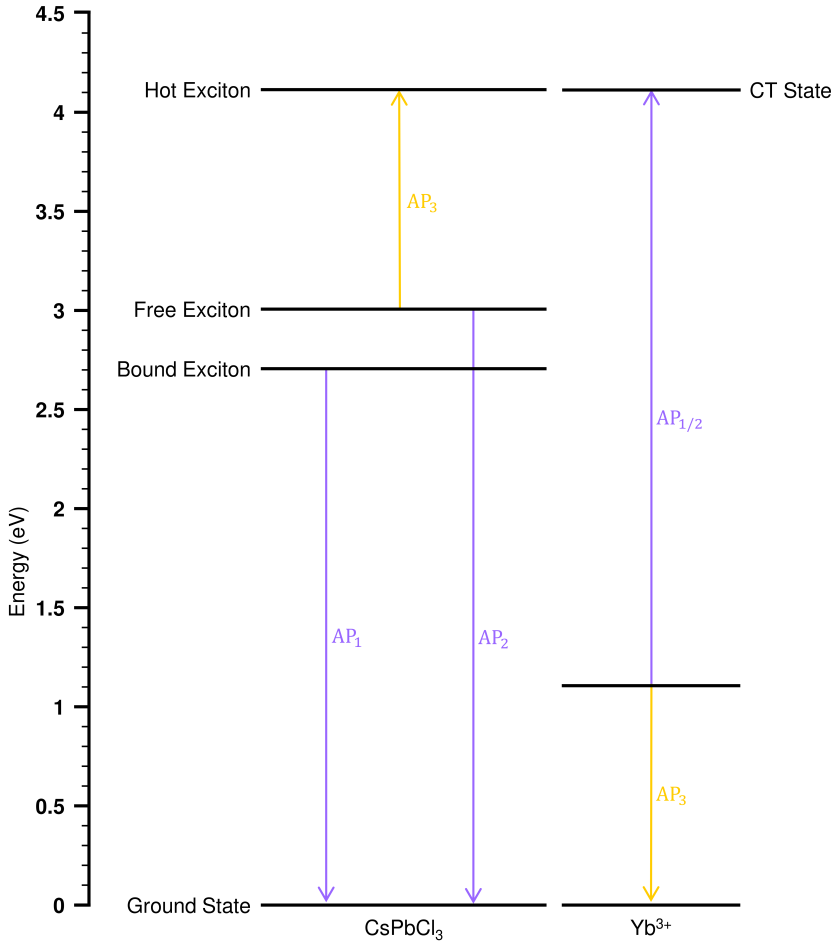

Figure 16 | Jablonski diagram depicting the three considered Auger processes that are modelled for the NIR luminescence saturation in $CsPbCl_3$:Yb^{3+}. AP_1 and AP_2, in which the energy of the respectively bound and free exciton is transferred to a readily excited ytterbium dopant to bring it in a charge transfer state, and AP_3, in which the energy of an excited dopant is transferred to a free exciton.

The model including the trap state, implicit pairs and different Auger processes then looks like the following:

Extended Saturation Model

Trap State & Explicit Pairs

$$\frac{dN_1}{dt} = k_{\mathrm{E}}N_0 - k_{\mathrm{EL}}N_1 - k_{\mathrm{T}}\underbrace{(A+B+C)}_{n_{\mathrm{V}_0}}N_1 + k_{\mathrm{D}}\underbrace{(D+E+F)}_{n_{\mathrm{V}_1}}N_0 - k_{\mathrm{AP}_2}\underbrace{(B+2C+E+2F)}_{n_{\mathrm{Yb}_1}}N_1 \tag{13.1}$$

$$\frac{d}{dt}(\mathrm{Yb_0\text{-}V_0\text{-}Yb_0}) = \frac{dA}{dt} = -k_{\mathrm{T}}AN_1 + k_{\mathrm{D}}DN_0 + k_{\mathrm{Yb}}B + k_{\mathrm{AP}_3}BN_1 \tag{13.2}$$

$$\frac{d}{dt}(\mathrm{Yb_1\text{-}V_0\text{-}Yb_0}) = \frac{dB}{dt} = -k_{\mathrm{T}}BN_1 + k_{\mathrm{D}}EN_0 + k_{\mathrm{Yb}}(2C-B) + k_{\mathrm{AP}_1}E + k_{\mathrm{AP}_3}(2C-B)N_1 \tag{13.3}$$

$$\frac{d}{dt}(\mathrm{Yb_1\text{-}V_0\text{-}Yb_1}) = \frac{dC}{dt} = -k_{\mathrm{T}}CN_1 + k_{\mathrm{D}}FN_0 - k_{\mathrm{Yb}}2C + k_{\mathrm{AP}_1}2F + k_{\mathrm{CET}}D - k_{\mathrm{AP}_3}2CN_1 \tag{13.4}$$

$$\frac{d}{dt}(\mathrm{Yb_0\text{-}V_1\text{-}Yb_0}) = \frac{dD}{dt} = +k_{\mathrm{T}}AN_1 - k_{\mathrm{D}}DN_0 + k_{\mathrm{Yb}}E - k_{\mathrm{CET}}D + k_{\mathrm{AP}_3}EN_1 \tag{13.5}$$

$$\frac{d}{dt}(\mathrm{Yb_1\text{-}V_1\text{-}Yb_0}) = \frac{dE}{dt} = +k_{\mathrm{T}}BN_1 - k_{\mathrm{D}}EN_0 + k_{\mathrm{Yb}}(2F-E) - k_{\mathrm{AP}_1}E + k_{\mathrm{AP}_3}(2F-E)N_1 \tag{13.6}$$

$$\frac{d}{dt}(\mathrm{Yb_1\text{-}V_1\text{-}Yb_1}) = \frac{dF}{dt} = +k_{\mathrm{T}}CN_1 - k_{\mathrm{D}}FN_0 - k_{\mathrm{Yb}}2F - k_{\mathrm{AP}_1}2F - k_{\mathrm{AP}_3}2FN_1 \tag{13.7}$$

$$2\underbrace{(A+B+C+D+E+F)}_{n_V} = n_{\mathrm{Yb}} \tag{13.8}$$

Equation 13.1 describes the change in the population of the free exciton through. Equations 13.2-13.4 describe the change in population of pairs with respectively none, one or both ytterbium dopants in their excited state, while the trap state is left empty, and equations 13.5-13.7 describe the change in population of pairs with respectively none, one or both ytterbium dopants in their excited state, while the trap state is occupied by a bound exciton. Equation 13.8 describes the condition that there is no change in the population of ytterbium dopants over time.

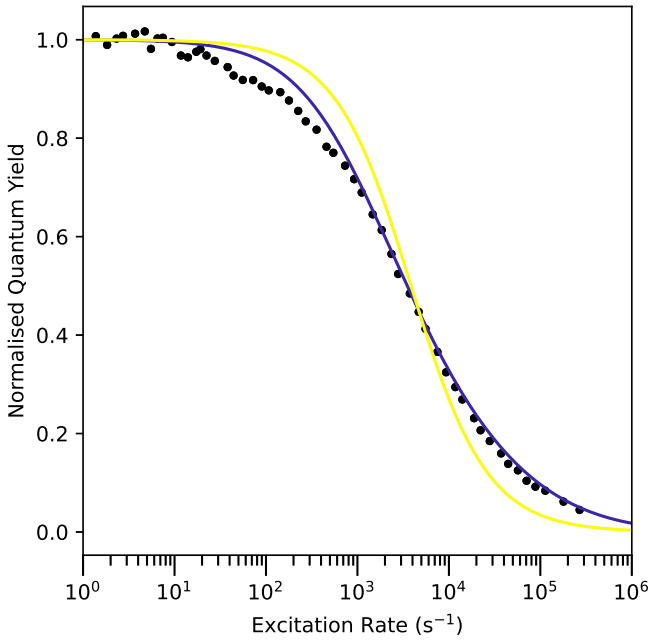

Figure 17 | NIR-QY as a function of the excitation rate in $CsPbCl_3$:Yb^{3+} (1.4%) NCs predicted for all considered Auger processes. The best fits for AP_1 and AP_2 predict the same behaviour and are in good agreement with experimental results (purple), whereas the best fit for AP_3 describes a saturation that depends too strongly on the excitation rate (yellow).

Figure 17 shows the measured and predicted NIR-luminescence saturation at room temperature. Three mechanisms are modelled in which the Auger process occurs with the energy transfer originating from the bound exciton ($k_{\mathrm{AP}_2} = k_{\mathrm{AP}_3} = 0,\ k_{\mathrm{AP}_1} \neq 0$), the free exciton ($k_{\mathrm{AP}_1} = k_{\mathrm{AP}_3} = 0,\ k_{\mathrm{AP}_2} \neq 0$) and the $^2F_{5/2}$ state ($k_{\mathrm{AP}_1} = k_{\mathrm{AP}_2} = 0,\ k_{\mathrm{AP}_3} \neq 0$). All models were fit for the Auger process rate constant against the data. For all other rate constants, experimental values previously obtained by the Gamelin research group were used. From these results we can conclude that the mechanism proposed by the Gamelin research group, in which the Auger process originates from the free exciton state (AP_2), is still valid when the trap state is considered in the model. In addition, a mechanism in which the saturation occurs through energy transfer from the bound exciton (AP_1) yields similar results. Similar to the conclusion made by the Gamelin research group, we conclude that a mechanism of saturation in which energy is transferred from an excited ytterbium dopant to an exciton can not explain the measured saturation.

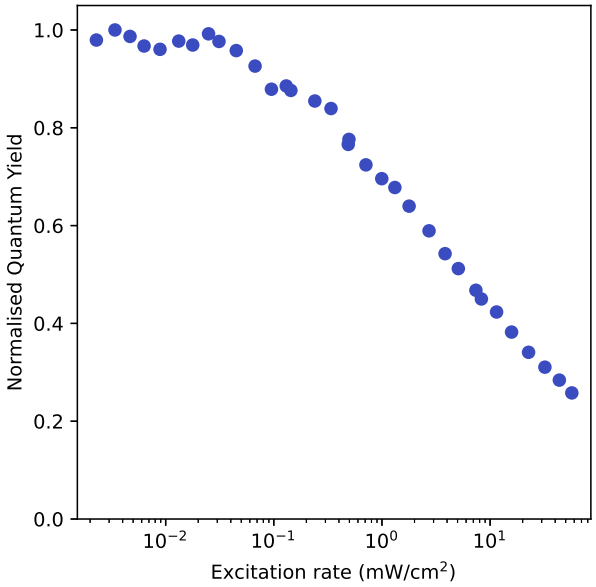

Figure 18 | Normalised NIR-QY of $CsPbCl_3$:Yb^{3+} (1.4%) NCs as a function of the fluence measured at $10\ \mathrm{K}$ excited with a 375 nm laser.

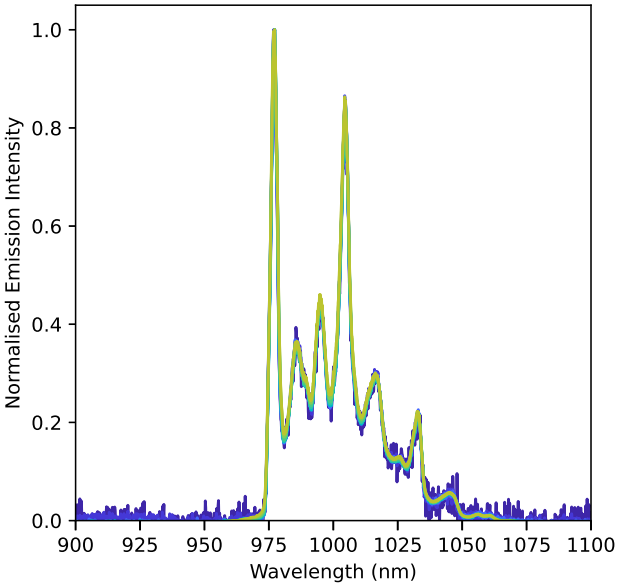

Figure 19 | Measured normalised NIR-emission spectra of $CsPbCl_3$:Yb^{3+} (1.4%) NCs at $10\ \mathrm{K}$ excited with a 375 nm laser with increasing excitation rates (purple to yellow).

Temperature Dependent NIR-luminescence Saturation

Similar to the NIR-luminescence intensity, we can model the expected change in saturation with temperature including and excluding a trap state in the quantum-cutting and saturation mechanism. Figure 18 shows the measured NIR-luminescence saturation measured at $10\ \mathrm{K}$. At this cryogenic temperature the saturation is still significantly present. We can therefore conclude that the process responsible for saturation is not phonon-assisted, or at most to a low degree. Therefore, the activation energy for the process must be low or (partly) assisted through a tunnelling effect.

Figure 19 shows the measured normalised emission spectra measured at $10\ \mathrm{K}$ at varying excitation rates. It is interesting to note that the spectra are identical, i.e. there is no change in the ratio between the different emission peaks. If different ytterbium species are responsible for the different emission peaks in the spectrum, Gamelins model predicts that a small difference in the quantum-cutting rate between two species would result in a weak change in the ratio of their emission due to experiencing different degrees of saturation. At $10\ \mathrm{K}$, if a second species has a quantum-cutting rate that is $10, 20, 30$ % faster, the emission rate ($n_{\mathrm{Yb}} k_{\mathrm{Yb}}$) between the species would respectively increase by $3.0, 5.4, 8.2$ % at $k_{\mathrm{E}} = 10^5\ \mathrm{s}^{-1}$. A difference in the Auger rate between species would not lead to different degrees of saturation if the Auger process occurs through energy transfer from the exciton to an excited ytterbium dopant. The absence of measuring a change in the emission spectra can have multiple explanations. The rate of quantum-cutting could be similar for different ytterbium species and fast excited state migration of excited ytterbium dopants causes rapid distribution of excited states among different species. Alternatively, the emission spectrum is not the result of different ytterbium species but of a single type. The latter explanation is unlikely, as the positions as well as the large amount of emission peaks can not be explained from radiative relaxation of Yb^{3+} from $^2F_{5/2}$ to $^2F_{7/2}$ in an octrahedral or orthorhombic coordination.[18]

Figure 20 shows the measured NIR-luminescence saturation measured at $10, 50, 125, 200$ and $275\ \mathrm{K}$. As the temperature increases from $10\ \mathrm{K}$ to $125\ \mathrm{K}$, the curve describing the saturation firstly shift to higher fluence, meaning that at higher temperatures a higher excitation rate leads to the same degree of saturation. Upon increasing the temperature further from 125 to $275\ \mathrm{K}$, the opposite occurs, the curve describing the saturation shift to lower fluence.

The model without a trap state predicts a continuous shift of the curve describing the saturation to higher fluence, see figure 21. Intuitively this can be understood from an increase in the quantum-cutting rate as well as the radiative decay rate of ytterbium with increasing temperature. The increase of both rates with increasing temperature causes the competitive

Auger process to occur less at higher temperatures. This modelled temperature dependent saturation is not in line with the measurement.

Figure 22 shows the predicted temperature dependent saturation for the model including a trap state with an energy difference of 100 meV with saturation occurring through AP_2. At cryogenic temperatures, the saturation is predicted to occur at higher fluence than at room temperature. Initially increasing the temperature from $10\ \mathrm{K}$ causes the saturation to occur at higher fluence, similar to the prediction without a trap state. As the temperature is increased further to 200 and $275\ \mathrm{K}$, the saturation occurs at lower fluence. As the temperature increases, the detrapping rate increases significantly, which causes the steady-state population of the free-exciton to increase and bound-exciton to decrease. In a model with saturation occurring through AP_2, an increase in the steady-state population of the free-exciton causes the Auger rate to increase. Simultaneously, a decrease in the steady-state population of the bound-exciton decreases the quantum-cutting rate. Therefore, a further increase in temperature towards room temperature causes saturation to occur at lower fluence. While the measurement does not match qualitatively with this model, the trend of an initial increase followed by a decrease of the fluence at which saturation occurs with increasing temperature is similar. We therefore conclude that a quantum-cutting mechanism that includes a trap state is more in line with our measurement.

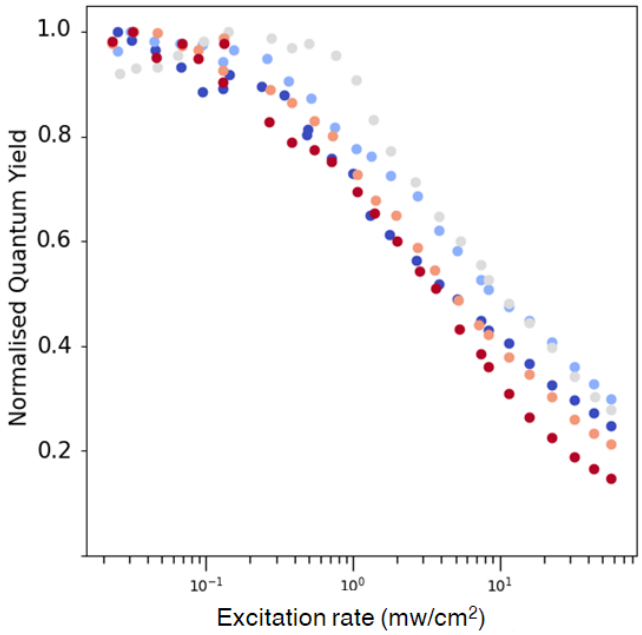

Figure 20 | Measured NIR-luminescence saturation at $10, 50, 125, 200$ and $275\ \mathrm{K}$ (blue to red) in $CsPbCl_3$:Yb^{3+} NCs excited with a 375 nm laser.

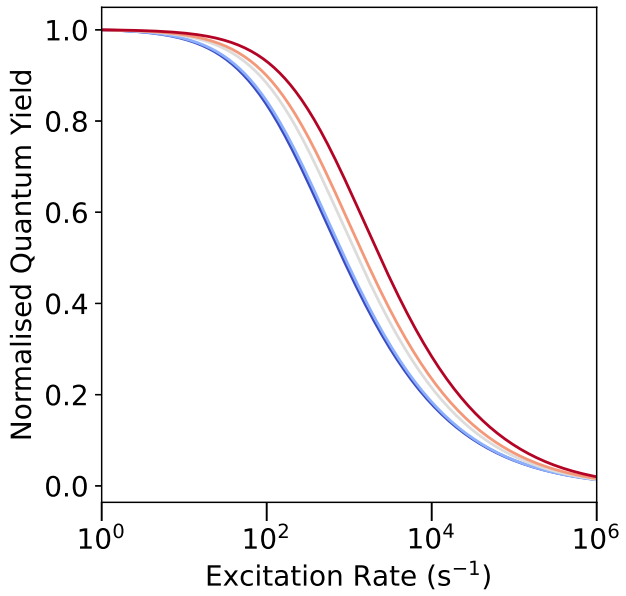

Figure 21 | Predicted NIR-luminescence saturation at $10, 50, 125, 200$ and 275 K (blue to red) in $CsPbCl_3:Yb^{3+}$ NCs for Gamelins model.

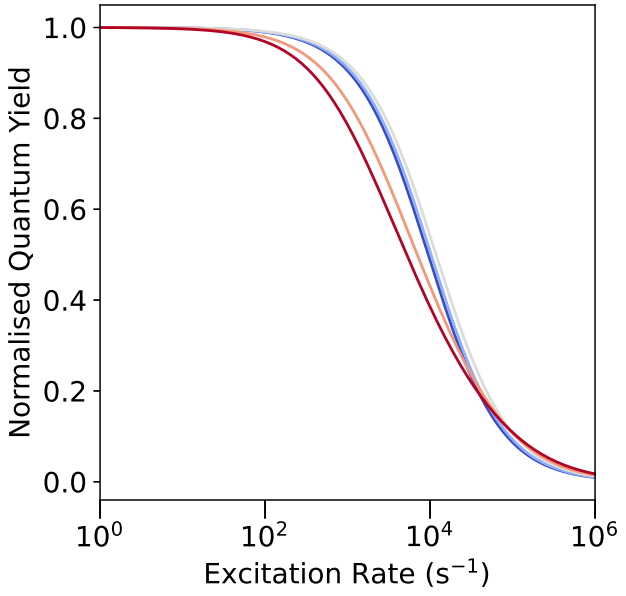

Figure 22 | Predicted NIR-luminescence saturation at $10, 50, 125, 200$ and 275 K (blue to red) in $CsPbCl_3:Yb^{3+}$ NCs for a model with an energy difference of 100 meV through AP_1.

Block-pulse Experiments

By using square-wave-modulated laser excitation, commonly referred to as a block-pulse, the rise and decay dynamics of luminescence can be measured in addition to the steady-state luminescence, which can provide insight in the saturation mechanisms of phosphors.[6] As we will show for $CsPbCl_3$:Yb^{3+}, the time dependent emission can also contain information about the excitation mechanism of a phosphor. Namely, if the quantum-cutting occurs through fixed pairs, the NIR-intensity can be stronger in the first few milliseconds after excitation, to which we will refer to as an overshoot. At high intensity of incident light, most pairs will have both ytterbium dopants in the excited state a few milliseconds after excitation. As the ytterbium dopants in their excited state decay through emission of a NIR-photon, with a decay rate on the order of milliseconds, ytterbium dopants are created that can not be re-excited through quantum-cutting until their adjacent ytterbium dopant has also returned to the ground state. Thus, quantum-cutting through fixed pairs results in a lower quantum-cutting efficiency during the steady state at high intensity of incident light, resulting in an overshoot of the NIR-luminescence intensity in the first few milliseconds of excitation. This behaviour is not expected for quantum-cutting through random pairs, as an ytterbium dopant in its ground state is not prevented from partaking quantum-cutting. Therefore, by measuring the time-dependent NIR-intensity, we can gain insight into the quantum-cutting mechanism.

We simplify the model discussed earlier by excluding the trap state, while still explicitly modelling the different energetic states of pairs. We neglect trapping and detrapping of the exciton as these processes are expected to be sufficiently fast at room temperature such that they do not affect the time dependent dynamics, which are dominated by the slow rise and decay dynamics of ytterbium. This simplified model then looks like the following:

Block-pulse Model

Excluding Energy Migration

$$\frac{dN_1}{dt} = k_{\mathrm{E}}N_0 - k_{\mathrm{EL}}N_1 - k_{\mathrm{CET}}AN_1 - k_{\mathrm{AP_2}}\underbrace{(B+2C)}_{n_{\mathrm{Yb_1}}}N_1$$

$$\frac{d}{dt}(\mathrm{Yb_0\text{-}Yb_0}) = \frac{dA}{dt} = +k_{\mathrm{Yb}}B - k_{\mathrm{CET}}AN_1 \tag{14.1}$$

$$\frac{d}{dt}(\mathrm{Yb_1\text{-}Yb_0}) = \frac{dB}{dt} = +k_{\mathrm{Yb}}\,(2C - B) \tag{14.2}$$

$$\frac{d}{dt}(\mathrm{Yb_1\text{-}Yb_1}) = \frac{dC}{dt} = -k_{\mathrm{Yb}}2C + k_{\mathrm{CET}}AN_1 \tag{14.3}$$

$$2(A+B+C) = n_{\mathrm{Yb}}$$

We can simulate square-wave-modulated laser excitation, in which the laser is pulsed for a fixed power and time, by making the excitation rate time dependent. The emission intensity is proportional to the number of excited state ytterbium dopants ($\mathrm{B}+2\mathrm{C}$). The predicted time dependent luminescence intensities from the model from Gamelin and through pairs are shown in figure 23. At high excitation powers, the predicted luminescence between the models differs significantly. As a result of incorporating the pairs explicitly in the model, an overshoot in luminescence intensity for the first few milliseconds is predicted (with respect to the steady-state luminescence intensity) at high excitation powers, which can be intuitively understood.

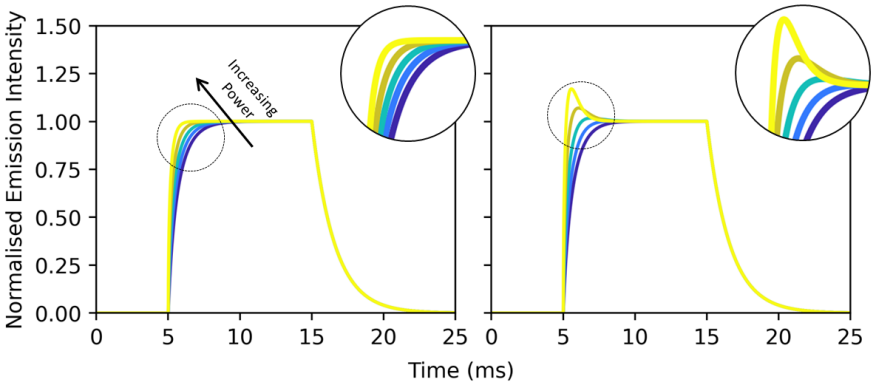

Figure 23 | Time dependent NIR-luminescence intensity, normalised by the steady state intensity (which scales with number of ytterbium dopants in their excited state), with implicit and explicit pairs (left and right respectively). Laser is on for $10\ \mathrm{ms}$ at $t = 5\ \mathrm{ms}$, with the excitation rate varying logarithmically from 10^4 to $10^6\ \mathrm{s}^{-1}$ (purple to yellow). $C_{\mathrm{Yb}^{3+}} = 1.4\%$ and diameter NCs is 11 nm.

Before excitation, every pair is in the ground state and can be excited such that directly after the inset of excitation mainly pairs with both dopants in their excited state are present (see figure 24, right). After inset of excitation, a high fraction of pairs will be have both dopants in the excited state. As some ytterbium dopant decay radiatively, pairs are formed with one ytterbium dopant in the ground state and one in the excited state (see figure 24, left). The steady-state luminescence can not be as strong as the initial luminescence intensity at high powers, due to the relatively high fraction of pairs with one dopant in the excited state and one in the ground state. Such pairs can not participate in quantum-cutting and thus prevent excitation of a large number of dopants in the ground state (inactive dopants). This is in contrast with a mechanism in which quantum-cutting occurs through random pairs, in which any combination of ground state ytterbium dopants can participate in quantum-cutting. So contrary to quantum-cutting through fixed pairs, dopants in their excited state do not complete prevent other dopants from participating in quantum-cutting. Measuring an overshoot in luminescence intensity would thus form proof for the existence of the proposed charge compensating ytterbium pairs, as well as proof for quantum-cutting occurring through these pairs.

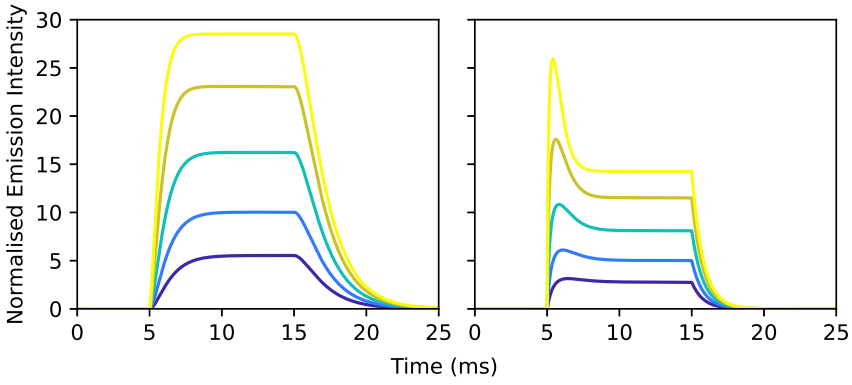

Figure 24 | Time dependent populations of pairs in different energetic states. left and right show pairs with respectively one and both ytterbium dopants in their excited state (respectively B and C in the model). Laser is on for $10\ \mathrm{ms}$ at $t = 5\ \mathrm{ms}$, with the excitation rate varying logarithmically from 10^4 to $10^6\ \mathrm{s}^{-1}$ (purple to yellow). $C_{\mathrm{Yb}^{3+}} = 1.4\%$ and diameter NCs is 11 nm.

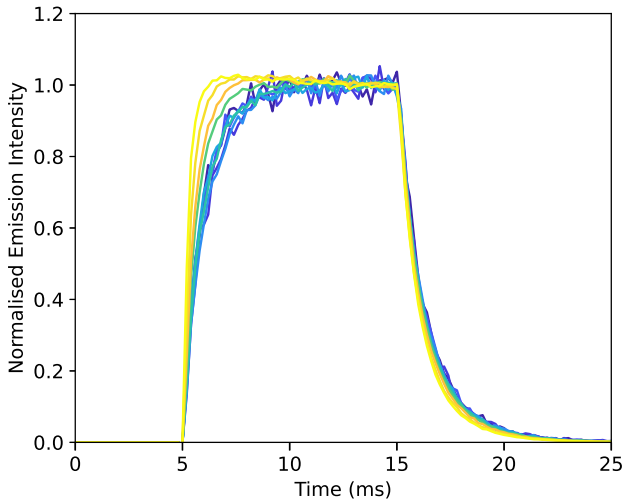

Figure 25 | Measured integrated time dependent NIR-emission of spin-coated $CsPbCl_3$:Yb^{3+} (<0.1%) NCs using a square-wave profile modulated 375 nm laser normalised to the highest plateau value. Laser is on for 10 ms at $t = 5$ ms, with the excitation rate varying logarithmically from approximately $2 \cdot 10^2$ to $5 \cdot 10^6$ s^{-1} (purple to yellow).

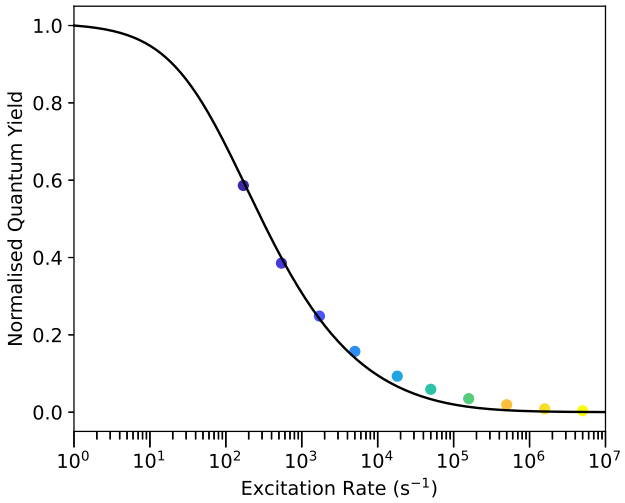

Figure 26 | Quantum yields against the excitation rate of spin-coated $CsPbCl_3$:Yb^{3+} (<0.1%) NCs using a square-wave profile modulated 375 nm laser normalised measured and fitted to the saturation predicted by the block-pulse model (Yb^{3+}%$= 0.1$%) including migration. (black). Colours correspond to measurements reported in figure 25.

Figure 25 shows the measured integrated NIR-emission of spin-coated $CsPbCl_3$:Yb^{3+} (<0.1%) NCs using a square-wave profile modulated 375 nm laser at different laser powers (purple to yellow) normalised to the highest plateau value. The rise and decay of the NIR-emission behave as expected, with the rise time becoming shorter with increasing power, whereas the decay time is independent of the power. No overshoot seems to be visible however, even at the highest power used experimentally.

There could be multiple reasons for the absence of such an overshoot; I) The maximum experimentally obtained excitation rate is to low, II) the quantum-cutting mechanism does not occur through CET to two ytterbium dopants that form a pair, III) excited state migration has a large influence on the overshoot. The first explanation is unlikely, as the maximum experimentally obtained excitation rate is close to 10^7 s^{-1}, which is well over the predicted required excitation rate. The obtained excitation rates were approximated by fitting the measured luminescence saturation to the model of Gamelin, using the NIR-emission intensities measured at plateau values. This is shown in figure 26. The second explanation is unlikely, as measurements of the concentration dependent NIR-QY and luminescence saturation provide evidence for quantum-cutting occurring through pairs.[7] We will now investigate how including excited state migration, the third explanation, effects the modelled results. It is expected that no overshoot is visible if excited state migration is sufficiently fast such that inactive ytterbium dopants are formed during the first few milliseconds after inset of excitation.

Including Excited State Migration

We now extend the model by including the possibility of excited state migration between ytterbium dopants. We find it significantly alters the predicted time-dependent emission intensity and provides insight for the experimental conditions to be able to measure an overshoot, namely the dopant concentration and excitation rate.

The migration rate of the excited state between two ytterbium dopants can be calculated by:

$$k_{\mathrm{M}} = \frac{C_{\mathrm{M}}}{r^6} \tag{15}$$

Where C_{M} is a material dependent constant and r is the distance between the dopants.[29] C_{M} for excited state migration between Yb^{3+} dopants is unknown for $CsPbCl_3$ as a host material, but has been calculated for fluorozirconate glass by the following equation:[29]

$$C_{\mathrm{M}} = \frac{6c}{(2\pi)^4 n^2} \frac{g^{\mathrm{l}}}{g^{\mathrm{u}}} \int \sigma_{\mathrm{emi}}(\lambda)\sigma_{\mathrm{abs}}(\lambda)d\lambda \tag{16}$$

Where c is the speed of light, n is the refractive index of the host lattice, g^{l} and g^{u} are respectively the degeneracy of the lower and upper energy levels of ytterbium, and σ_{emi} and σ_{abs} are respectively the normalised absorption and emission spectral cross sections.[29] The value of C_{M} will differ for $CsPbCl_3$:Yb^{3+} due to differences in the absorption and emission of Yb^{3+} and the refractive index of the host. The effect of difference in absorption and emission are difficult to account for but are expected to be small due to the weak dependence of the host on the f-orbitals and is therefore not corrected for. We do account for the difference in refractive index by recalculating the migration rate constant using equation 16 with the refractive indexes reported in literature.[30,31] With an estimate for the migration rate constant, the average migration rate for a single dopant in a NC can be calculated by considering the migration rates of all dopants with all other dopants:

$$\langle k_{\mathrm{M}} \rangle = \frac{C_{\mathrm{M}}}{n_{\mathrm{Yb}}} \left(\sum_{i=0}^{n_{\mathrm{Yb}}} \sum_{j \neq i}^{n_{\mathrm{Yb}}} \frac{1}{r_{\mathrm{ij}}^6} - \frac{1}{r_{\mathrm{pair}}^6} \right) \tag{17}$$

Where $\mathrm{n_{Yb}}$ is the number of dopants, $\mathrm{r_{ij}}$ is the distance between two dopants, and $\mathrm{r_{pair}}$ is the distance between two dopants within the same pair. Migration between dopants within the same pair do not affect the populations of the different energetic states of pairs, which is accounted for by the negative term. Using a Monte Carlo simulation (See Methods for a detailed description), we generate many different NCs with a fixed size and number of dopant pairs and calculate the average migration rate over all dopants in all NCs. With an estimate for the migration rate, migration can be incorporated into the model:

Block-pulse Model

Including Energy Migration

$$\frac{dN_1}{dt} = k_{\mathrm{E}} N_0 - k_{\mathrm{EL}} N_1 - k_{\mathrm{CET}} A N_1 - k_{\mathrm{AP_2}} \underbrace{(B + 2C)}_{n_{\mathrm{Yb_1}}} N_1$$

$$\frac{d}{dt}(\mathrm{Yb_0\text{-}Yb_0}) = \frac{dA}{dt} = +k_{\mathrm{Yb}} B - k_{\mathrm{CET}} A N_1 - 8\langle k_{\mathrm{M}} \rangle \frac{AC}{n_{\mathrm{Yb}}} + 2\langle k_{\mathrm{M}} \rangle \frac{B^2}{n_{\mathrm{Yb}}}$$

$$\frac{d}{dt}(\mathrm{Yb_1\text{-}Yb_0}) = \frac{dB}{dt} = +k_{\mathrm{Yb}} (2C - B) + 16\langle k_{\mathrm{M}} \rangle \frac{AC}{n_{\mathrm{Yb}}} - 4\langle k_{\mathrm{M}} \rangle \frac{B^2}{n_{\mathrm{Yb}}}$$

$$\frac{d}{dt}(\mathrm{Yb_1\text{-}Yb_1}) = \frac{dC}{dt} = -k_{\mathrm{Yb}} 2C + k_{\mathrm{CET}} A N_1 - 8\langle k_{\mathrm{M}} \rangle \frac{AC}{n_{\mathrm{Yb}}} + 2\langle k_{\mathrm{M}} \rangle \frac{B^2}{n_{\mathrm{Yb}}}$$

$$2(A + B + C) = n_{\mathrm{Yb}}$$

We only consider migration of the $^2F_{5/2}$ excited state from pairs with both dopants in their excited state to pairs with both dopants in the ground state and its reverse process, as these are the only migration processes concomitant with a change in the number of pairs in a given energy state (see figure 27).

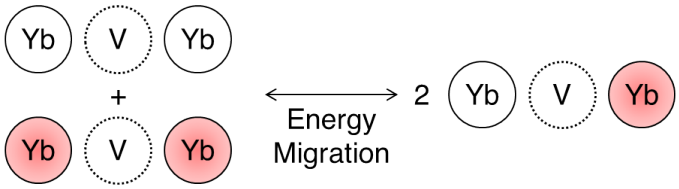

Figure 27 | Schematic representation of the energy migration processes included in the model: energy migrating from pairs with both ytterbium dopants in their excited state to pairs with both dopants in the ground state and the reverse process.

The constants in the equations are a result of considering the number of dopants that can contribute to the process, the number of pairs in a given energy state that are formed or lost as a result of excited state migration, and the division by the number of pairs ($n_{\mathrm{Yb}}/2$). As the calculation for the average migration rate considers the interaction with every other dopant, the division by the number of pairs is required to account for the probability of having a pair to which the energy migrates in the correct energy state. For example, the term $+16\langle k_{\mathrm{M}}\rangle \frac{AC}{n_{\mathrm{Yb}}}$ describes the increase in the population of pairs with one ytterbium dopant in its excited state (B) due to energy migration from a pair with both dopants in their excited state (C) to a pair with both dopants in the ground state (A). C has 2 dopants which can transfer their energy, A has 2 dopants which can accept the energy. This process creates 2 pairs with energy state B. Taking the product between these constants and dividing by the number of pairs ($n_{\mathrm{Yb}}/2$) results in the constant $+16$.

Figure 28 shows the normalised overshoot intensity as a function of the number of pairs structures occupying a nanocrystal and the excitation rate excluding and including migration. From these results, it is clear that migration would significantly alter the predicted time-dependent luminescence such that an overshoot in the luminescence intensity is only visible at low dopant concentrations ($< 0.3\%$ Yb^{3+}), in which case the migration rate is low, and at high powers. For these reasons, the measurements were done on a sample with a low dopant concentration ($< 0.1\%$ Yb^{3+}) and measured to high powers ($\sim 5 \cdot 10^7$ s^{-1}).

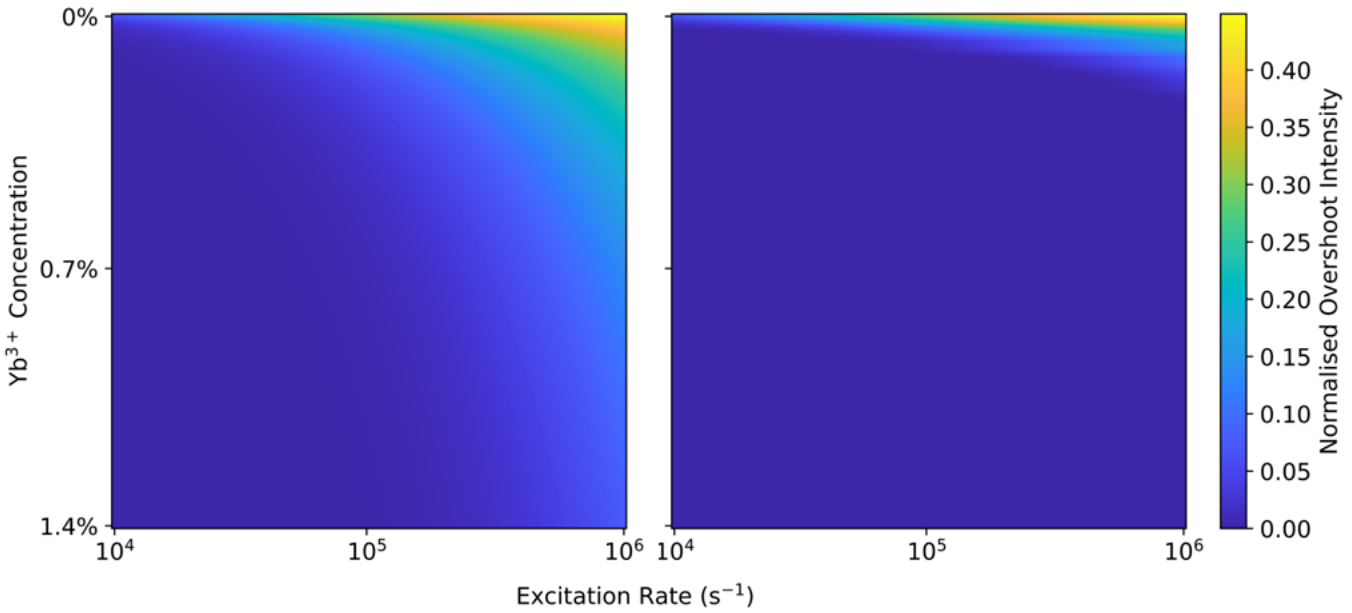

Figure 28 | Normalised overshoot intensity as function of number of pairs and excitation rate predicted by the model excluding and including excited state migration (left and right respectively). $C_{\mathrm{M}} = 2.36 \cdot 10^9$ $\mathrm{\AA}^6$ s^{-1} and diameter NCs is 11 nm. 100 dopants corresponds to a doping concentration of $\sim 1.4\%$.

Saturation Model based on Weiss' Research

The Weiss Research Group recently investigated the mechanism behind quantum-cutting in $CsPbCl_3$:Yb^{3+} NCs though transient absorption measurements and came to the conclusion that energy transfer is mediated through a charge transfer intermediate.[15] Energy transfer from the exciton to an Yb^{3+} dopant would occur by two consecutive steps: electron transfer from the conduction band within picoseconds, creating an ytterbium dopant in its divalent state, followed by hole transfer from the valence band accompanied with quantum-cutting within nanoseconds. It is interesting to note that the creation of a divalent ytterbium dopant is part of the quantum-cutting mechanism proposed by Weiss, whereas it is part of the luminescence saturation mechanism proposed by Gamelin.[7] The proposal of its requirement to obtain quantum-cutting properties seems to be in contrast with the proposal of its effect on the quantum-cutting efficiency with increasing light intensity. We therefore explore a new model in which we attempt to unify both proposals, in which the creation of a divalent ytterbium dopant is part of the mechanism for both quantum-cutting and luminescence saturation.

Electron transfer (ET) to a ground state ytterbium dopant ($\mathrm{Yb_0}$) creates a divalent ytterbium dopant ($\mathrm{Yb_2}$). Hole transfer (HT) can then either lead to the creation of two excited ytterbium dopants ($\mathrm{Yb_1}$) or one depending on the energetic state of the pair. In this model we assume hole transfer is accompanied with quantum-cutting if the other dopant that is part of the pair is in its ground state ($\mathrm{HT_1}$), whereas only a single new excited state dopant is created after hole transfer if the other dopant that is part of the pair is in an excited or divalent state ($\mathrm{HT_2}$). The model then looks like the following:

Saturation Model

Through Divalent Ytterbium Dopants

$$\frac{dN_1}{dt} = k_{\mathrm{E}}N_0 - k_{\mathrm{EL}}N_1 - k_{\mathrm{ET}}N_1\,(2A + B + D) \tag{19.1}$$

$$\frac{d}{dt}(\mathrm{Yb_0\text{-}Yb_0}) = \frac{dA}{dt} = k_{\mathrm{Yb}}B - k_{\mathrm{ET}}N_1 2A \tag{19.2}$$

$$\frac{d}{dt}(\mathrm{Yb_1\text{-}Yb_0}) = \frac{dB}{dt} = k_{\mathrm{Yb}}(2C - B) - k_{\mathrm{ET}}N_1 B \tag{19.3}$$

$$\frac{d}{dt}(\mathrm{Yb_1\text{-}Yb_1}) = \frac{dC}{dt} = k_{\mathrm{HT_1}}D - k_{\mathrm{Yb}}2C + k_{\mathrm{HT_2}}E \tag{19.4}$$

$$\frac{d}{dt}(\mathrm{Yb_2\text{-}Yb_0}) = \frac{dD}{dt} = k_{\mathrm{ET}}N_1(2A - D) - k_{\mathrm{HT_1}}D + k_{\mathrm{Yb}}E \tag{19.5}$$

$$\frac{d}{dt}(\mathrm{Yb_2\text{-}Yb_1}) = \frac{dE}{dt} = k_{\mathrm{ET}}N_1 B - k_{\mathrm{Yb}}E + k_{\mathrm{HT_2}}(2F - E) \tag{19.6}$$

$$\frac{d}{dt}(\mathrm{Yb_2\text{-}Yb_2}) = \frac{dF}{dt} = k_{\mathrm{ET}}N_1 D - k_{\mathrm{HT_2}}2F \tag{19.7}$$

$$2\,(A + B + C + D + E + F) = n_{\mathrm{Yb}} \tag{19.8}$$

We approximate the reported rates of electron and hole transfer with 10^{12} and 10^9 s^{-1} respectively.[15] The predicted saturation (figure 29, yellow) is not in line with the measured saturation (black), which sets in at much lower light intensity. We therefore model the possibility of two distinct rates for hole transfer accompanied with quantum-cutting ($\mathrm{HT_1}$) and hole transfer with single energy transfer ($\mathrm{HT_2}$). If the latter process can occur faster, saturation occurs at lower light intensity, but reaches a plateau level at a quantum yield of 0.5. This plateau value is reached because effectively every exciton transfers its energy to a single ground state ytterbium dopant through $\mathrm{HT_2}$. A drop in the quantum cutting rate is visible at an excitation rate of $\sim 10^5$ s^{-1} as excited state depletion of ytterbium dopants causes a further decrease in the quantum-cutting efficiency at higher light intensities. All modelled predictions of the saturation are in disagreement with the measured saturation. We therefore come to the conclusion that this model in which both quantum-cutting and luminescence saturation occurs through the presence of divalent ytterbium atoms can not explain the observed luminescence saturation, instead, additional pathways through which energy is lost are needed.

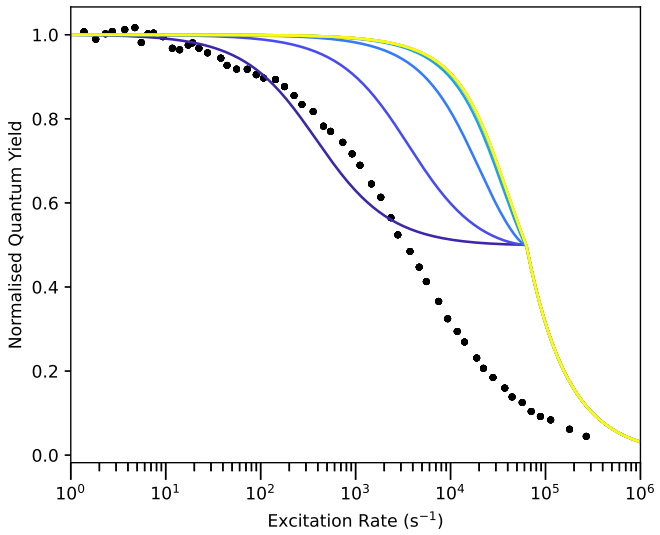

Figure 29 | Predicted NIR-luminescence saturation in $CsPbCl_3:Yb^{3+}$ (1.4%) NCs based on the quantum-cutting mechanism suggested by Weiss against data of Gamelin with k_{HT_2} ranging logarithmically from 10^3 to 10^9 s^{-1} (purple through yellow).

CONCLUSIONS

We have shown that the measured temperature dependent NIR-QY of $CsPbCl_3:Yb^{3+}$ NCs in the lower power regime is in qualitative agreement with a model in which quantum-cutting occurs through direct energy transfer between the exciton and ytterbium dopants. A model that includes an intermediate trap state in the quantum-cutting mechanism would significantly change the predicted behaviour in the temperature dependent NIR-QY, which is in bad agreement with the experimental results. Similar to previous results, distinct different emission peaks are visible at cryogenic temperature, which were previously attributed to different species of ytterbium emitters with different emission spectra. We have shown that the emission spectrum at 10 K does not change to measurable degree when varying the excitation power over five orders of magnitude, suggesting that NIR-emission stems from multiple species through having similar quantum-cutting rates and/or fast excited state migration between the species. We also conclude that the model proposed by Gamelin can not account for the linear behaviour of the exciton quantum yield with the excitation rate, as this would also be affected by saturation. Additionally, we have measured the temperature dependent NIR-luminescence saturation, which follows qualitatively different behaviour than a model without a trap state predicts. Increasing the temperature from ~ 10 to ~ 125 K initially causes the saturation to occur at higher powers, but as the sample is further heated towards room temperature, saturation occurs at lower powers. This behaviour is qualitatively more in line with a model with a trap state. Lastly, we have shown that if quantum-cutting occurs through fixed pairs, the NIR-luminescence intensity should exceed the steady-state value in the first few milliseconds after inset of excitation. Time-resolved measurements in combination with square-wave-profile laser excitation show no sign of measuring such an overshoot. These results suggest quantum-cutting occurs through random pairs, in which any combination of ytterbium dopants can participate in quantum-cutting. We also show through modelling how the absence of an overshoot could be the result of having not the right experimental conditions, such as a low dopant concentration, high power, and low influence of excited state migration. For these reasons we can not rule out a quantum-cutting mechanism involving fixed pairs.

■ OUTLOOK

With the conflicting results of involvement of an intermediate trap state in the quantum-cutting mechanism, as well as the Weiss research group recently providing evidence for involvement of a divalent ytterbium dopants, further research is needed to elucidate the mechanism responsible for the quantum-cutting and luminescence saturation properties of $CsPbCl_3:Yb^{3+}$. Measurements on the QY of the exciton as a function of the excitation rate could provide additional evidence for or disproof the mechanism proposed to cause NIR-luminescence saturation. Temperature dependent transient absorption measurements would provide insight in the temperature dependence of trapping, which can be compared with the temperature dependent trapping model. Evidence for pairwise quantum-cutting could be found by measuring the NIR-luminescence saturation in $CsPbCl_3:Yb^{3+}/La^{3+}$ with a fixed ytterbium concentration and a varying lanthanum concentration. For collaborative quantum-cutting, the amount of available quantum-cutting pairs remains the same such that NIR-luminescence saturation should remain unaffected by different concentrations of La^{3+}. This is in contrast for pairwise quantum-cutting, which would experience saturation at lower excitation rates because the concentration of quantum-cutting pairs would be reduced through the formation of inactive pairs, which would contain one lanthanum dopant paired with an ytterbium dopant that can not partake in quantum cutting.

■ ACKNOWLEDGEMENTS

Jur de Wit is thanked for his assistance in setting up the cryo-experiments, as well as Thomas van Swieten for assistance in working with the Andor spectroscope, and Sander Vonk for advice and help on working with optical setups. Mark Mangnus and Freddy Rabouw are thanked for their helpful advice and criticism throughout the research project.

■ REFERENCES

1. Van der Zwaan, B. & Arbl, A. Prospects for PV: a Learning Curve Analysis. *Sol Energy* **74,** 19–31 (2013).
2. Zhang, Q. & Huang, X. Recent Progress in Quantum Cutting Phosphors. *Prog. Mater. Sci.* **55,** 353–427 (2010).
3. Pan, G. *et al.* Doping Lanthanide into Perovskite Nanocrystals: Highly Improved and Expanded Optical Properties. *Nano Lett.* **17,** 8005–8011 (2017).
4. Zhou, D. *et al.* Cerium and Ytterbium Codoped Halide Perovskite Quantum Dots: A Novel and Efficient Downconverter for Improving the Performance of Silicon Solar Cells. *Adv. Mater.* **29,** 1704149 (2017).
5. Milstein, T. J., Kroupa, D. M. & Gamelin, D. R. Picosecond Quantum Cutting Generates Photoluminescence Quantum Yields Over 100% in Ytterbium-Doped $CsPbCl_3$ Nanocrystals. *Nano Lett.* **18,** 3792–3799 (2018).
6. Van de Haar, M. A. *et al.* Saturation Mechanisms in Common LED Phosphors. *ACS Photonics* **8,** 1784–1793 (2021).
7. Erickson, C. S., Crane, M. J., Milstein, T. J. & Gamelin, D. R. Photoluminescence Saturation in Quantum-Cutting Yb^{3+}-Doped $CsPb(Cl_{1-x}Br_x)_3$ Perovskite Nanocrystals: Implications for Solar Downconversion. *J. Phys. Chem. C* **123,** 12474–12484 (2019).
8. Kroupa, D. M., Roh, J. Y., Milstein, T. J., Creutz, S. E. & Gamelin, D. R. Quantum-Cutting Ytterbium-Doped $CsPb(Cl_{1-x}Br_x)_3$ Perovskite Thin Films with Photoluminescence Quantum Yields over 190%. *ACS Energy Lett.* **3,** 2390–2395 (2018).
9. Cohen, T. A. *et al.* Quantum-cutting Yb^{3+}-doped Perovskite Nanocrystals for Monolithic Bilayer Luminescent Solar Concentrators. *J. Mater. Chem. A* **7,** 9279–9288 (2019).
10. Crane, M. J. *et al.* Single-Source Vapor Deposition of Quantum-Cutting Yb^{3+}:$CsPb(Cl_{1-x}Br_x)_3$ and Other Complex Metal-Halide Perovskites. *ACS Appl. Energy Mater.* **2,** 4560–4565 (2019).
11. Crane, M. J., Kroupa, D. M. & Gamelin, D. R. Detailed-Balance Analysis of Yb^{3+}:$CsPb(Cl_{1-x}Br_x)_3$ Quantum-Cutting Layers for High-Efficiency Photovoltaics under Real-World Conditions. *Energy and Environ. Sci.* **12,** 2486–2495 (2019).
12. Henling, L. M. & McPherson, G. L. EPR spectra of magnetically coupled pairs of Gd^{3+} ions in crystals of $CsMgCl_3$, $CsMgBr_3$, and $CsCdBr_3$. *Phys. Rev. B* **16,** 4756–4760 (1977).
13. Li, X. *et al.* Mechanism for the Extremely Efficient Sensitization of Yb^{3+} Luminescence in $CsPbCl_3$ Nanocrystals. *J. Phys. Chem. Lett.* **10,** 487–492 (2019).
14. Ding, N. *et al.* Extremely efficient quantum-cutting Cr^{3+}, Ce^{3+}, Yb^{3+} tridoped perovskite quantum dots for highly enhancing the ultraviolet response of Silicon photodetectors with external quantum efficiency exceeding 70%. *Nano Energy* **78,** 105278 (2020).
15. Chang, W. J., Irgen-Gioro, S., Padgaonkar, S., López-Arteaga, R. & Weiss, E. A. Photoredox-Mediated Sensitization of Lanthanide Dopants by Perovskite Nanocrystals. *ACS* **125,** 25634–25642 (2021).
16. Mello Donegá, C. D. Nanoparticles: Workhorses of Nanoscience. (Springer, 2014).
17. Weller, M. Inorganic Chemistry (Oxford University Press, 2014).
18. Roh, J. Y. D. *et al.* Yb^{3+} Speciation and Energy-transfer Dynamics in Quantum-cutting Yb^{3+}-doped $CsPbCl_3$ Perovskite Nanocrystals and Single Crystals. *Phys. Rev. Mater.* **4,** 105405 (2020).
19. Stefanski, M., Ptak, M., Sieradzki, A. & Strek, W. Optical Characterization of Yb^{3+}:$CsPbCl_3$ Perovskite Powder. *Chem. Eng. J.* **408,** 127347 (2021).
20. Withnall, R. & Silver, J. Physics of light emission from rare-earth doped phosphors (Springer, 2012).
21. Pandey, N., Kumar, A. & Chakrabarti, S. Investigation of the structural, electronic, and optical properties of Mn-doped $CsPbCl_3$: theory and experiment. *ACS Appl. Mater.* **9,** 29556–29565 (2019).
22. Sebastian, M. *et al.* Excitonic Emissions and Above-band-gap Luminescence in the Single-crystal Perovskite Semiconductors $CsPbBr_3$ and $CsPbCl_3$. *Phys. Rev. B* **92,** 235210 (2015).
23. Shi, J. *et al.* Identification of High-temperature Exciton States and their Phase-dependent Trapping Behaviour in Lead Halide Perovskites. *Energy Environ. Sci.* **11,** 1460–1469 (2018).
24. Lao, X. *et al.* Luminescence and Thermal Behaviors of Free and Trapped excitons in Cesium Lead Halide Perovskite Nanosheets. *Nanoscale* **10,** 9949–9956 (2018).
25. Huang, H. *et al.* Ytterbium-Doped $CsPbCl_3$ Quantum Cutters for Near-Infrared Light-Emitting Diodes. *ACS Appl. Mater. Interfaces* **13,** 34561–34571 (2021).
26. Guo, P. *et al.* Polar Fluctuations in Metal Halide Perovskites Uncovered by Acoustic Phonon Anomalies. *ACS Energy Lett.* **2,** 2463–2469 (2018).
27. Diroll, B. T., Zhou, H. & Schaller, R. D. Low-Temperature Absorption, Photoluminescence, and Lifetime of $CsPbX_3$ (X = Cl, Br, I) Nanocrystals. *Adv. Funct. Mater.* **28,** 1800945 (2018).

28. Ma, J. *et al.* Insights into the Local Structure of Dopants, Doping Efficiency, and Luminescence Properties of Lanthanide-doped $CsPbCl_3$ Perovskite Nanocrystals. *J. Mater. Chem. C* **7,** 3037–3048 (2019).

29. Da Vila, L. D., Gomes, L. & Tarelho, L. V. G. Mechanism of the Yb–Er Energy Transfer in Fluorozirconate Glass. *J. Appl. Phys.* **93,** 3873 (2003).

30. Harrington, J. A. Infrared Fibers and Their Applications. *SPIE Press* (2004).

31. Padmavathy, R., Amudhavalli, A., Rajeswarapalanichamy, R. & Iyakutti, K. Electronic and Optical Properties of Cubic Perovskites $CsPbCl_{3y}I_y$ (y = 0, 1, 2, 3). *Z. Naturforsch.* **74,** 905–913 (2019).